ELSEVIER

Comput. Methods Appl. Mech. Engrg. 184 (2000) 241–267

Computer methods in applied mechanics and engineering

www.elsevier.com/locate/cma

A distributed Lagrange multiplier/fictitious domain method for the simulation of flow around moving rigid bodies: application to particulate flow

Roland Glowinski [a], Tsorng-Whay Pan [a,*], Todd I. Hesla [b], Daniel D. Joseph [b], Jacques Periaux [c]

[a] *Department of Mathematics, University of Houston, Houston, TX 77204-3476, USA*

[b] *Department of Aerospace Engineering & Mechanics, University of Minnesota, 107 Ackerman Hall, 110 Union Street, Minneapolis, MN 55455, USA*

[c] *Dassault Aviation, 78, Quai Marcel Dassault, 92314 Saint-Cloud, France*

Abstract

In this article we discuss the application of a Lagrange multiplier based fictitious domain method to the numerical simulation of incompressible viscous flow modeled by the Navier–Stokes equations around moving rigid bodies; the rigid body motion is due to hydrodynamical forces and gravity. The solution method combines finite element approximations, time discretization by operators splitting and conjugate gradient algorithms for the solution of the linearly constrained quadratic minimization problems coming from the splitting method. We conclude this article by the presentation of numerical results concerning the simulation of an incompressible viscous flow around a NACA0012 airfoil with a fixed center, but free to rotate, then the sedimentation of circular cylinders in 2-D channels, and finally the sedimentation of spherical balls in cylinders with square cross-sections.

Keywords: Particulate flow; Fictitious domain methods; Navier–Stokes equations; Liquid–solid mixtures; Rayleigh–Taylor instabilities

1. Introduction

Fictitious domain methods (some authors prefer to call them *domain embedding* methods) is a general term which covers in fact a large variety of solution methods for partial differential equations. Glowinski et al. discussed, in [1–3], fictitious domain methods based on *boundary supported Lagrange multipliers* to enforce *Dirichlet boundary conditions* and on regular structured meshes (which were not boundary fitted) over a simple shape auxiliary domain (the fictitious domain). These methods, initially developed for the solution of linear elliptic problems, have also been applied, as shown in the above references, to the solution of nonlinear time dependent problems, such as the variational inequalities modeling the flow of a viscous–plastic medium in a pipe, Ginzburg–Landau equations, and the Navier–Stokes equations modeling incompressible viscous unsteady flow. For the simulation of flow around moving rigid bodies, whose motion is known a priori, Glowinski et al. [4–6] have coupled the above boundary distributed multiplier method with time discretization by operator splitting à la Marchuk–Yanenko and with L^2-projection technique which forces the incompressibility condition; the resulting methodology is robust, stable and easy to implement and parallelize.

* Corresponding author.
E-mail address: pan@math.uh.edu (T.-W. Pan).

0045-7825/00/$ - see front matter
PII: S0045-7825(99)00230-3

In this article, we consider the numerical simulation of *incompressible viscous flow* around *moving rigid bodies* when the rigid body motion is caused by *hydrodynamical forces* and given external forces, such as gravity; let us mention several applications: fluidized beds, sedimentation, blood flow around artificial heart valves, store separation. The method of choice is a *distributed Lagrange multiplier/fictitious domain method* which consists to fill the moving bodies by the surrounding fluid and impose a rigid body motion to the fluid filling the regions previously occupied by the rigid bodies; then one relaxes the rigid body motion constraint by using distributed Lagrange multipliers and obtains a flow problem over the entire region. This approach is quite different from the one in Refs. [4–6], which is concerned with the case where the rigid body motion is known a priori. An advantage of the fictitious domain method discussed here is that we do not need to generate a new mesh at each time step, immediately after updating the positions of the rigid bodies. This is a very important issue since for 3-D particulate flow, generating meshes for simulating fluid-rigid body interactions is still a major problem and seems to require powerful parallel computers (see, e.g., Ref. [7]). If one uses the fictitious domain methods, described in this article, one just needs a very simple mesh for the rigid bodies which can be generated very quickly. Moreover, we do not need to compute the hydrodynamical forces explicitly, since the interaction between fluid and rigid bodies is implicitly modeled by the global variational formulation at the foundation of the present methodology. This methodology has been applied to simulate the flow around a NACA0012 airfoil which has a fixed center of mass, but is free to rotate under the effect of hydrodynamical forces, and the motion of sedimenting rigid bodies in 2-D and 3-D channels and cylinders.

Let us mention that non-Lagrange multiplier based fictitious domain methods have been used by Peskin and his collaborators [8–10] to simulate incompressible viscous flow in regions with elastic moving boundaries and by LeVeque [11,12] for elliptic problems with discontinuous coefficients and singular sources and Stokes flow with elastic boundaries or surface tension.

2. A model problem and its fictitious domain formulation

Let $\Omega \subset \mathbb{R}^d (d = 2, 3$; see Fig. 1 for a particular case where $d = 2)$ be a space region; we suppose that Ω is filled with a *Newtonian viscous incompressible* fluid (of *density* ρ_f and *viscosity* ν_f) and contains a moving rigid body B. The fluid flow is modeled by the following *Navier–Stokes equations*

$$\rho_f \left[\frac{\partial \mathbf{u}}{\partial t} + (\mathbf{u} \cdot \nabla)\mathbf{u} \right] = \rho_f \mathbf{g} + \nabla \cdot \boldsymbol{\sigma} \quad \text{in } \Omega \setminus \overline{B(t)}, \tag{2.1}$$

$$\nabla \cdot \mathbf{u} = 0 \quad \text{in } \Omega \setminus \overline{B(t)}, \tag{2.2}$$

$$\mathbf{u}(\mathbf{x}, 0) = \mathbf{u}_0(\mathbf{x}) \quad \forall \mathbf{x} \in \Omega \setminus \overline{B(0)} \ \ (\text{with } \nabla \cdot \mathbf{u}_0 = 0), \tag{2.3}$$

$$\mathbf{u} = \mathbf{g}_0 \quad \text{on } \Gamma, \tag{2.4}$$

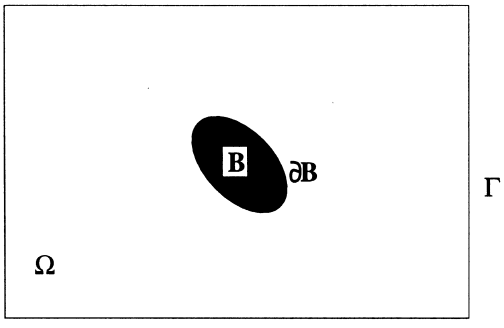

Fig. 1. An example of 2-D flow region with one rigid body.

to be completed by the boundary conditions on the boundary $\partial B(t)$ of $B(t)$, given hereafter (see (2.9)). In (2.1)–(2.4), the *stress-tensor* $\boldsymbol{\sigma}$ is defined by

$$\boldsymbol{\sigma} = -p\mathbf{I} + \nu_{\mathrm{f}}(\nabla\mathbf{u} + \nabla\mathbf{u}^t), \tag{2.5}$$

$\mathbf{u}\left(= \{u_i\}_{i=1}^d\right)$ and p denote, as usual, velocity and pressure, respectively; the viscosity ν_{f} positive, $\mathbf{g}$ the gravity and $\mathbf{x}(= \{x_i\}_{i=1}^d)$ is the generic point of $\mathbb{R}^d$, and

$$(\mathbf{u}\cdot\nabla)\mathbf{u} = \left\{ \sum_{j=1}^{d} u_j \frac{\partial u_i}{\partial x_j} \right\}_{i=1}^{d}.$$

From the rigid body motion of B, $\mathbf{g}_0$ has to satisfy $\int_\Gamma \mathbf{g}_0 \cdot \mathbf{n}\,\mathrm{d}\Gamma = 0$, where $\mathbf{n}$ denotes the unit vector of the outward normal at Γ (we suppose the *no-slip* condition on ∂B). In the following, we shall use, if necessary, the notation $\phi(t)$ for the function $\mathbf{x} \to \varphi(\mathbf{x}, t)$.

Assuming that the rigid body B does not touch Γ, its motion is described by the following *Euler's equations* (an almost direct consequence of Newton's laws of motion)

$$M\frac{\mathrm{d}\mathbf{V_G}}{\mathrm{d}t} = M\mathbf{g} + \mathbf{F}, \tag{2.6}$$

$$\mathbf{I}\frac{\mathrm{d}\boldsymbol{\omega}}{\mathrm{d}t} - \mathbf{I}\boldsymbol{\omega}\times\boldsymbol{\omega} = \mathbf{T}, \tag{2.7}$$

$$\frac{\mathrm{d}\mathbf{G}}{\mathrm{d}t} = \mathbf{V_G}, \tag{2.8}$$

where $\mathbf{V_G}$ is the *translation velocity* of the rigid body $B, \boldsymbol{\omega}$ the *angular velocity* of B, M the mass of the rigid body, $\mathbf{I}$ is *inertia tensor* of the rigid body at $\mathbf{G}$ and $\mathbf{G}$ being the center of mass of B. As already mentioned $\mathbf{g}$ denotes gravity, while $\mathbf{F}$ and $\mathbf{T}$ are the resultant and the torque at $\mathbf{G}$ of the hydrodynamical forces acting on B, respectively. The *boundary condition* on ∂B is given by

$$\mathbf{u} = \mathbf{V_G} + \boldsymbol{\omega}\times\mathbf{Gx} \quad \forall \mathbf{x} \in \partial B. \tag{2.9}$$

The *force* $\mathbf{F}$ and *torque* $\mathbf{T}$ imposed on the rigid body by the fluid are described as follows:

$$\mathbf{F} = \int_{\partial B} \boldsymbol{\sigma}\mathbf{n}\,\mathrm{d}\gamma, \tag{2.10}$$

$$\mathbf{T} = \int_{\partial B} \mathbf{Gx}\times(\boldsymbol{\sigma}\mathbf{n})\,\mathrm{d}\gamma, \tag{2.11}$$

where $\mathrm{d}\gamma = d(\partial B)$, $\mathbf{x}$ is the generic point of ∂B and $\mathbf{n}$ is the pointing outward unit normal vector on ∂B. In order to treat possible *collisions* between B and Γ (collisions between particles will be addressed later on), we substitute to the *momentum equation* in (2.6) the following modified one

$$M\frac{\mathrm{d}\mathbf{V_G}}{\mathrm{d}t} = M\mathbf{g} + \mathbf{F} + \mathbf{F}^r, \tag{2.12}$$

where $\mathbf{F}^r$ is a *lubrication force* (see [13,14]) imposed on B by Γ (in those parts of Γ that B cannot cross).

Remark 2.1. *If B is made of an homogeneous material of density ρ_{s}, we have*

$$M = \rho_{\mathrm{s}}\int_B \mathrm{d}\mathbf{x}, \tag{2.13}$$

$$\mathbf{I} = \begin{pmatrix} I_{11} & -I_{12} & -I_{13} \\ -I_{12} & I_{22} & -I_{23} \\ -I_{13} & -I_{23} & I_{33} \end{pmatrix}, \tag{2.14}$$

where, in (2.13) *and* (2.14), $d\mathbf{x} = dx_1dx_2dx_3$ *and*

$$I_{11} = \rho_s \int_B (x_2^2 + x_3^2)\, d\mathbf{x}, \quad I_{22} = \rho_s \int_B (x_3^2 + x_1^2)\, d\mathbf{x}, \quad I_{33} = \rho_s \int_B (x_1^2 + x_2^2)\, d\mathbf{x}, \tag{2.15}$$

$$I_{12} = I_{21} = \rho_s \int_B x_1x_2\, d\mathbf{x}, \quad I_{23} = I_{32} = \rho_s \int_B x_2x_3\, d\mathbf{x}, \quad I_{31} = I_{13} = \rho_s \int_B x_3x_1\, d\mathbf{x} \tag{2.16}$$

with the usual simplification for 2-*D phenomena*.

Remark 2.2. *If the flow-rigid body motion is* 2-*D, or if B is a spherical ball made of an homogeneous material, then the quadratic term* $\mathbf{I}\boldsymbol{\omega} \times \boldsymbol{\omega}$ *vanishes in* (2.7).

Remark 2.3. *We have to complete the Euler's equations* (2.6)–(2.8) *by initial conditions, typical ones being*

$$\mathbf{V}_\mathbf{G}(0) = \mathbf{V}^0, \tag{2.17}$$

$$\boldsymbol{\omega}(0) = \boldsymbol{\omega}^0, \tag{2.18}$$

$$\mathbf{G}(0) = \mathbf{G}^0. \tag{2.19}$$

To obtain a variational formulation for problem (2.1)–(2.4), (2.7)–(2.12) and (2.17)–(2.19), we define first the following functional spaces

$$V_{\mathbf{g}_0}(t) = \{\mathbf{v} \mid \mathbf{v} \in (H^1(\Omega \setminus \overline{B(t)}))^d,\ \mathbf{v} = \mathbf{g}_0(t) \quad \text{on} \quad \Gamma,\ \mathbf{v} = \mathbf{V}_\mathbf{G}(t) + \boldsymbol{\omega}(t) \times \mathbf{G}(t)\mathbf{x} \text{ on } \partial B(t)\}, \tag{2.20}$$

$$\begin{aligned} V_0(t) = &\{\{\mathbf{v}, \mathbf{Y}, \boldsymbol{\theta}\} \mid \mathbf{v} \in (H^1(\Omega \setminus \overline{B(t)}))^d,\ \mathbf{v} = \mathbf{0} \text{ on } \Gamma,\ \mathbf{v} = \mathbf{Y} + \boldsymbol{\theta} \times \mathbf{G}(t)\mathbf{x} \text{ on } \partial B(t), \\ &\text{with } \mathbf{Y} \in \mathbb{R}^d,\ \boldsymbol{\theta} \in \mathbb{R}^3\}, \end{aligned} \tag{2.21}$$

$$L_0^2(\Omega \setminus \overline{B(t)}) = \left\{ q \mid q \in L^2(\Omega \setminus \overline{B(t)}),\ \int_{\Omega \setminus \overline{B(t)}} q\, d\mathbf{x} = 0 \right\}. \tag{2.22}$$

In (2.20) and (2.21) we have $\boldsymbol{\omega}(t) = \{\omega_i(t)\}_{i=1}^3$ and $\boldsymbol{\theta} = \{\theta_i\}_{i=1}^3$ if $d = 3$, while $\boldsymbol{\omega}(t) = \{0, 0, \omega(t)\}$ and $\boldsymbol{\theta} = \{0, 0, \theta\}$ if $d = 2$.

Applying the *virtual power* principle to system (2.1)–(2.4), (2.7)–(2.12) and (2.17)–(2.19) yields the following *variational formulation*:

$$\begin{aligned} &\text{For a.e. } t > 0,\ \text{find } \{\mathbf{u}(t), p(t), \mathbf{V}_\mathbf{G}(t), \mathbf{G}(t), \boldsymbol{\omega}(t)\} \quad \text{such that} \\ &\mathbf{u}(t) \in V_{\mathbf{g}_0}(t),\ p(t) \in L_0^2(\Omega \setminus \overline{B(t)}),\ \mathbf{V}_\mathbf{G}(t) \in \mathbb{R}^d,\ \mathbf{G}(t) \in \mathbb{R}^d,\ \boldsymbol{\omega}(t) \in \mathbb{R}^3 \end{aligned} \tag{2.23}$$

and

$$\begin{aligned} &\rho_f \int_{\Omega \setminus \overline{B(t)}} \frac{\partial \mathbf{u}}{\partial t} \cdot \mathbf{v}\, d\mathbf{x} + \rho_f \int_{\Omega \setminus \overline{B(t)}} (\mathbf{u} \cdot \nabla)\mathbf{u} \cdot \mathbf{v}\, d\mathbf{x} - \int_{\Omega \setminus \overline{B(t)}} p\nabla \cdot \mathbf{v}\, d\mathbf{x} + 2\nu_f \int_{\Omega \setminus \overline{B(t)}} \mathbf{D}(\mathbf{u}) : \mathbf{D}(\mathbf{v})\, d\mathbf{x} \\ &\quad + \left(M \frac{d\mathbf{V}_\mathbf{G}}{dt} - M\mathbf{g} - \mathbf{F}^r \right) \cdot \mathbf{Y} + (\mathbf{I}\frac{d\boldsymbol{\omega}}{dt} - \mathbf{I}\boldsymbol{\omega} \times \boldsymbol{\omega}) \cdot \boldsymbol{\theta} = \rho_f \int_{\Omega \setminus \overline{B(t)}} \mathbf{g} \cdot \mathbf{v}\, d\mathbf{x} \quad \forall \{\mathbf{v}, \mathbf{Y}, \boldsymbol{\theta}\} \in V_0(t), \end{aligned} \tag{2.24}$$

$$\int_{\Omega \setminus \overline{B(t)}} q\nabla \cdot \mathbf{u}(t)\, d\mathbf{x} = 0 \quad \forall q \in L^2(\Omega \setminus \overline{B(t)}), \tag{2.25}$$

$$\frac{d\mathbf{G}}{dt} = \mathbf{V}_\mathbf{G}, \tag{2.26}$$

$$\mathbf{u}(\mathbf{x}, 0) = \mathbf{u}_0(\mathbf{x}) \quad \forall \mathbf{x} \in \Omega \setminus \overline{B(0)} \quad (\text{with } \nabla \cdot \mathbf{u}_0 = 0), \tag{2.27}$$

$$\mathbf{V}_{\mathbf{G}}(0)=\mathbf{V}^0,\quad \boldsymbol{\omega}(0)=\boldsymbol{\omega}^0,\quad \mathbf{G}(0)=\mathbf{G}^0 \tag{2.28}$$

within, (2.23)–(2.28), $\boldsymbol{\omega}(t)$ and $\boldsymbol{\theta}$ as in (2.20) and (2.21), $\mathbf{D}(\mathbf{v})=(\nabla\mathbf{v}+\nabla\mathbf{v}^t)/2$; also, in (2.24), we have used the following notation

$$\mathbf{a}\cdot\mathbf{b}=\sum_{i=1}^{d}a_ib_i\ \ \forall\mathbf{a}\quad\text{and}\quad\mathbf{b}\in\mathbb{R}^d,$$

$$\mathbf{A}:\mathbf{B}=\sum_{i=1}^{d}\sum_{j=1}^{d}a_{ij}b_{ij}\ \ \forall\mathbf{A}=(a_{i,j})_{1\leqslant i,j\leqslant d}\quad\text{and}\quad\mathbf{B}=(b_{ij})_{1\leqslant i,j\leqslant d}.$$

To the best of our knowledge, the above variational formulation was introduced by Hesla [15]. Hu [16] also developed a similar variational formulation and combined it with an *arbitrary Lagrange–Euler* (ALE) technique to simulate the flow-motion of 2-D solid–liquid mixtures in a vertical channel with unstructured grid.

In order to obtain an *equivalent fictitious domain* formulation, we shall proceed as follows:

(i) First, we fill the rigid body B by the surrounding fluid (i.e., embed $\Omega\setminus\overline{B(t)}$ in Ω).

(ii) Next, we correct (2.34) taking (i) into account.

(iii) Finally, we relax the rigid body motion constraint by using a *distributed Lagrange multiplier* and obtain a fictitious domain formulation over the entire region.

Let us implement (i) and (ii). If we fill B with a fluid of density ρ_{f} and if we suppose that this fluid has the same rigid body motion as B itself, we have for the fluid velocity inside B.

$$\mathbf{u}(\mathbf{x},t)=\mathbf{V}_{\mathbf{G}}(t)+\boldsymbol{\omega}(t)\times\mathbf{G}\mathbf{x}\quad\forall\mathbf{x}\in B(t). \tag{2.29}$$

Suppose now that $\{\mathbf{v},\mathbf{Y},\boldsymbol{\theta}\}$ verifies

$$\{\mathbf{v},\mathbf{Y},\boldsymbol{\theta}\}\in\tilde{V}_0(t)=\left\{\{\mathbf{v},\mathbf{Y},\boldsymbol{\theta}\}\mid\left\{\mathbf{v}\mid_{\Omega\setminus\overline{B(t)}},\mathbf{Y},\boldsymbol{\theta}\right\}\in V_0(t),\mathbf{v}(\mathbf{x},t)=\mathbf{Y}+\boldsymbol{\theta}\times\mathbf{G}(t)\mathbf{x}\ \forall\mathbf{x}\in B(t)\right\}. \tag{2.30}$$

We have then, if B is made of an homogeneous material of density ρ_{s} (an assumption that we shall make from now on),

$$\rho_{\mathrm{f}}\left(\int_{B(t)}\frac{\partial\mathbf{u}}{\partial t}\cdot\mathbf{v}\,\mathrm{d}\mathbf{x}+\int_{B(t)}(\mathbf{u}\cdot\nabla)\mathbf{u}\cdot\mathbf{v}\,\mathrm{d}\mathbf{x}\right)=(\rho_{\mathrm{f}}/\rho_{\mathrm{s}})\left[M\frac{\mathrm{d}\mathbf{V}_{\mathbf{G}}}{\mathrm{d}t}\cdot\mathbf{Y}+\left(\mathbf{I}\frac{\mathrm{d}\boldsymbol{\omega}}{\mathrm{d}t}-\mathbf{I}\boldsymbol{\omega}\times\boldsymbol{\omega}\right)\cdot\boldsymbol{\theta}\right]. \tag{2.31}$$

We also have

$$\rho_{\mathrm{f}}\int_{B(t)}\mathbf{v}\cdot\mathbf{g}\,\mathrm{d}\mathbf{x}=(\rho_{\mathrm{f}}/\rho_{\mathrm{s}})M\mathbf{g}\cdot\mathbf{Y}\quad\forall\{\mathbf{v},\mathbf{Y},\boldsymbol{\theta}\}\in\tilde{V}_0(t), \tag{2.32}$$

$$\nabla\cdot\mathbf{v}=0\text{ in }B(t)\quad\forall\{\mathbf{v},\mathbf{Y},\boldsymbol{\theta}\}\in\tilde{V}_0(t), \tag{2.33}$$

and, if $\mathbf{u}$ verifies (2.29),

$$\nabla\cdot\mathbf{u}=0\text{ in }B(t)\quad\text{and}\quad\mathbf{D}(\mathbf{u})=\mathbf{0}\text{ in }B(t). \tag{2.34}$$

Combining (2.29)–(2.34) with (2.23)–(2.28) yields the following variation of the virtual-power based formulation:

For a.e. $t>0$, find $\{\mathbf{u}(t),p(t),\mathbf{V}_{\mathbf{G}}(t),\mathbf{G}(t),\boldsymbol{\omega}(t)\}$ such that

$$\mathbf{u}(t)\in W_{\mathbf{g}_0}(t),\ \ p(t)\in L^2_0(\Omega),\ \ \mathbf{V}_{\mathbf{G}}(t)\in\mathbb{R}^d,\ \ \mathbf{G}(t)\in\mathbb{R}^d,\ \ \boldsymbol{\omega}(t)\in\mathbb{R}^3 \tag{2.35}$$

and

$$\rho_f \int_\Omega \frac{\partial \mathbf{u}}{\partial t} \cdot \mathbf{v}\, d\mathbf{x} + \rho_f \int_\Omega (\mathbf{u} \cdot \nabla)\mathbf{u} \cdot \mathbf{v}\, d\mathbf{x} - \int_\Omega p \nabla \cdot \mathbf{v}\, d\mathbf{x} + 2\nu_f \int_\Omega \mathbf{D}(\mathbf{u}) : \mathbf{D}(\mathbf{v})\, d\mathbf{x}$$
$$+ (1 - \rho_f/\rho_s)\left[M \frac{d\mathbf{V_G}}{dt} \cdot \mathbf{Y} + \left(\mathbf{I}\, \frac{d\boldsymbol{\omega}}{dt} - \mathbf{I}\boldsymbol{\omega} \times \boldsymbol{\omega} \right) \cdot \boldsymbol{\theta} \right] - \mathbf{F}^r \cdot \mathbf{Y}$$
$$= \rho_f \int_\Omega \mathbf{g} \cdot \mathbf{v}\, d\mathbf{x} + (1 - \rho_f/\rho_s) M \mathbf{g} \cdot \mathbf{Y} \quad \forall \{\mathbf{v}, \mathbf{Y}, \boldsymbol{\theta}\} \in \tilde{V}_0(t), \tag{2.36}$$

$$\int_\Omega q \nabla \cdot \mathbf{u}(t) d\mathbf{x} = 0 \quad \forall q \in L^2(\Omega), \tag{2.37}$$

$$\frac{d\mathbf{G}}{dt} = \mathbf{V_G}, \tag{2.38}$$

$$\mathbf{u}(\mathbf{x}, t) = \mathbf{V_G}(t) + \boldsymbol{\omega}(t) \times \mathbf{G}(t)\mathbf{x} \quad \forall \mathbf{x} \in B(t), \tag{2.39}$$

$$\mathbf{V_G}(0) = \mathbf{V}^0, \quad \boldsymbol{\omega}(0) = \boldsymbol{\omega}^0, \quad \mathbf{G}(0) = \mathbf{G}^0, \tag{2.40}$$

$$\mathbf{u}(\mathbf{x}, 0) = \mathbf{u}_0(\mathbf{x}) \ \ \forall \mathbf{x} \in \Omega \setminus \overline{B(t)} \quad \text{and} \quad \mathbf{u}(\mathbf{x}, 0) = \mathbf{V}^0 + \boldsymbol{\omega}^0 \times \mathbf{G}^0 \mathbf{x} \ \ \forall \mathbf{x} \in \overline{B(0)}, \tag{2.41}$$

with, in formulation (2.35)–(2.41), space $W_{\mathbf{g}_0}(t)$ defined by

$$W_{\mathbf{g}_0}(t) = \{\mathbf{v} \mid \mathbf{v} \in (H^1(\Omega))^d, \ \mathbf{v} = \mathbf{g}_0(t) \text{ on } \Gamma\} \tag{2.42}$$

(and the usual simplification of $\boldsymbol{\omega}$ and $\boldsymbol{\theta}$ if $d = 2$).

In order to relax the *rigid body motion condition* (2.39), we introduce a *Lagrange multiplier*, $\boldsymbol{\lambda}$, so that $\boldsymbol{\lambda}(t) \in \Lambda(t) = (H^1(B(t)))^d$; we obtain then the following *fictitious domain formulation with distributed Lagrange multipliers*

For a.e. $t > 0$, find $\{\mathbf{u}(t), p(t), \mathbf{V_G}(t), \mathbf{G}(t), \boldsymbol{\omega}(t), \boldsymbol{\lambda}(t)\}$ such that
$$\mathbf{u}(t) \in W_{\mathbf{g}_0}(t), \ \ p(t) \in L^2_0(\Omega), \ \ \mathbf{V_G}(t) \in \mathbb{R}^d, \ \ \mathbf{G}(t) \in \mathbb{R}^d, \ \ \boldsymbol{\omega}(t) \in \mathbb{R}^3, \ \ \boldsymbol{\lambda}(t) \in \Lambda(t) \tag{2.43}$$

and

$$\rho_f \int_\Omega \frac{\partial \mathbf{u}}{\partial t} \cdot \mathbf{v}\, d\mathbf{x} + \rho_f \int_\Omega (\mathbf{u} \cdot \nabla)\mathbf{u} \cdot \mathbf{v}\, d\mathbf{x} - \int_\Omega p \nabla \cdot \mathbf{v}\, d\mathbf{x} + 2\nu_f \int_\Omega \mathbf{D}(\mathbf{u}) : \mathbf{D}(\mathbf{v}) d\mathbf{x}$$
$$- (\boldsymbol{\lambda}, \mathbf{v} - \mathbf{Y} - \boldsymbol{\theta} \times \mathbf{G}\mathbf{x})_{\Lambda(t)} + (1 - \rho_f/\rho_s)\left[M \frac{d\mathbf{V_G}}{dt} \cdot \mathbf{Y} + \left(\mathbf{I} \frac{d\boldsymbol{\omega}}{dt} - \mathbf{I}\boldsymbol{\omega} \times \boldsymbol{\omega} \right) \cdot \boldsymbol{\theta} \right] - \mathbf{F}^r \cdot \mathbf{Y}$$
$$= (1 - \rho_f/\rho_s) M \mathbf{g} \cdot \mathbf{Y} + \rho_f \int_\Omega \mathbf{g} \cdot \mathbf{v}\, d\mathbf{x} \quad \forall \mathbf{v} \in (H^1_0(\Omega))^d \quad \forall \mathbf{Y} \in \mathbb{R}^d \quad \forall \boldsymbol{\theta} \in \mathbb{R}^3, \tag{2.44}$$

$$\int_\Omega q \nabla \cdot \mathbf{u}(t)\, d\mathbf{x} = 0 \quad \forall q \in L^2(\Omega), \tag{2.45}$$

$$\frac{d\mathbf{G}}{dt} = \mathbf{V_G}, \tag{2.46}$$

$$(\boldsymbol{\mu}, \mathbf{u}(t) - \mathbf{V_G}(t) - \boldsymbol{\omega}(t) \times \mathbf{G}(t)\mathbf{x})_{\Lambda(t)} = 0 \quad \forall \boldsymbol{\mu} \in \Lambda(t), \tag{2.47}$$

$$\mathbf{V_G}(0) = \mathbf{V}^0, \quad \boldsymbol{\omega}(0) = \boldsymbol{\omega}^0, \quad \mathbf{G}(0) = \mathbf{G}^0, \tag{2.48}$$

$$\mathbf{u}(\mathbf{x}, 0) = \mathbf{u}_0(\mathbf{x}) \ \ \forall \mathbf{x} \in \Omega \setminus \overline{B(0)} \quad \text{and} \quad \mathbf{u}(\mathbf{x}, 0) = \mathbf{V}^0 + \boldsymbol{\omega}^0 \times \mathbf{G}^0 \mathbf{x} \ \ \forall \mathbf{x} \in \overline{B(0)}, \tag{2.49}$$

the two most natural choices for $(\cdot,\cdot)_{\Lambda(t)}$ are

$$(\boldsymbol{\mu},\mathbf{v})_{\Lambda(t)}=\int_{B(t)}(\boldsymbol{\mu}\cdot\mathbf{v}+\delta^2\nabla\boldsymbol{\mu}:\nabla\mathbf{v})\mathrm{d}\mathbf{x}\quad\forall\boldsymbol{\mu}\text{ and }\mathbf{v}\in\Lambda(t),\tag{2.50}$$

$$(\boldsymbol{\mu},\mathbf{v})_{\Lambda(t)}=\int_{B(t)}(\boldsymbol{\mu}\cdot\mathbf{v}+\delta^2\mathbf{D}(\boldsymbol{\mu}):\mathbf{D}(\mathbf{v}))\mathrm{d}\mathbf{x}\quad\forall\boldsymbol{\mu}\text{ and }\mathbf{v}\in\Lambda(t),\tag{2.51}$$

with δ a *characteristic length* (the diameter of B, for example).

The variational formulation (2.43)–(2.49) is due to the first two authors.

Remark 2.4. *Since, in* (2.44), $\mathbf{u}$ *is divergence free and satisfies Dirichlet boundary conditions of* Γ, *we have*

$$2\int_\Omega\mathbf{D}(\mathbf{u}):\mathbf{D}(\mathbf{v})\,\mathrm{d}\mathbf{x}=\int_\Omega\nabla\mathbf{u}:\nabla\mathbf{v}\,\mathrm{d}\mathbf{x}\quad\forall\mathbf{v}\in(H_0^1(\Omega))^d,$$

a substantial simplification, indeed, from a computational point of view, *which is another plus for the fictitious domain approach used here.*

Remark 2.5. *Using High Energy Physics terminology, the multiplier* $\boldsymbol{\lambda}$ *can be viewed as a gluon whose role is to force the rigidity of* B.

3. Finite element approximation

For simplicity, we assume that $\Omega\subset\mathbb{R}^2$ (i.e., $d=2$) and is polygonal; we have then $\boldsymbol{\omega}(t)=\{0,0,\omega(t)\}$ and $\boldsymbol{\theta}=\{0,0,\theta\}$ with $\omega(t)$ and $\theta\in\mathbb{R}$. Concerning the *space approximation* of problem (2.43)–(2.49) by a finite element method, we shall proceed as follows:

With h a *space discretization step* we introduce a finite element triangulation $\mathscr{T}_h$ of $\bar{\Omega}$ and then $\mathscr{T}_{2h}$ a triangulation twice coarser (in practice we should construct $\mathscr{T}_{2h}$ first and then $\mathscr{T}_h$ by joining the midpoints of the edges of $\mathscr{T}_{2h}$, dividing thus, each triangle of $\mathscr{T}_{2h}$ into 4 similar subtriangles, as shown in Fig. 2, below).

We define the following finite dimensional spaces which approximate $W_{\mathbf{g}_0}(t)$, $(H_0^1(\Omega))^2$, $L^2(\Omega)$, $L_0^2(\Omega)$, respectively:

$$W_{\mathbf{g}_{0h}}(t)=\Big\{\mathbf{v}_h\mid\mathbf{v}_h\in(C^0(\bar{\Omega}))^2,\ \mathbf{v}_h\mid_T\in P_1\times P_1\ \forall T\in\mathscr{T}_h,\ \mathbf{v}_h\mid_\Gamma=\mathbf{g}_{0h}(t)\Big\},\tag{3.1}$$

$$W_{0h}=\Big\{\mathbf{v}_h\mid\mathbf{v}_h\in(C^0(\bar{\Omega}))^2,\ \mathbf{v}_h\mid_T\in P_1\times P_1\ \forall T\in\mathscr{T}_h,\ \mathbf{v}_h\mid_\Gamma=0\Big\},\tag{3.2}$$

$$L_h^2=\Big\{q_h\mid q_h\in C^0(\bar{\Omega}),\ q_h\mid_T\in P_1\ \forall T\in\mathscr{T}_{2h}\Big\},\quad L_{0h}^2=\{q_h\mid q_h\in L_h^2,\ \int_\Omega q_h\,\mathrm{d}\mathbf{x}=0\}\tag{3.3}$$

in (3.1)–(3.3), $\mathbf{g}_{0h}(t)$ is an approximation of $\mathbf{g}_0(t)$ verifying $\int_\Gamma\mathbf{g}_{0h}(t)\cdot\mathbf{n}\,\mathrm{d}\Gamma=0$ and P_1 is the space of the polynomials in two variables of degree $\leqslant 1$.

Fig. 2. Subdivision of a triangle of $\mathscr{T}_{2h}$.

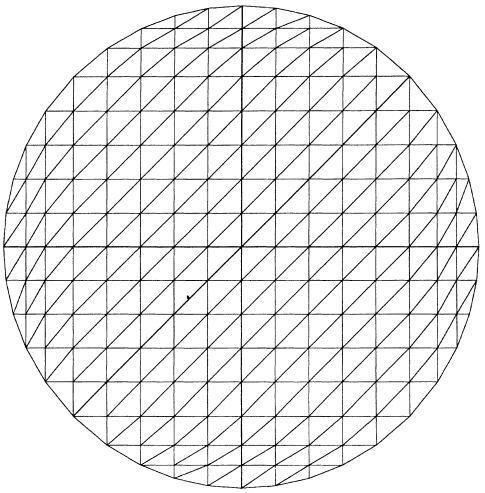

Fig. 3. Triangulation of a disk.

Let $\overline{B_h(t)}$ be a polygonal domain inscribed in $\overline{B(t)}$ and $\mathscr{T}_{B_h(t)}$ be a finite element triangulation of $\overline{B_h(t)}$, like the one shown in Fig. 3, where B is a disk.

Then, a finite dimensional space approximating $\Lambda(t)$ is

$$\Lambda_h(t) = \left\{ \boldsymbol{\mu}_h \mid \boldsymbol{\mu}_h \in (C^0(\overline{B_h(t)}))^2,\ \boldsymbol{\mu}_h \mid_T \in P_1 \times P_1\ \forall T \in \mathscr{T}_{B_h(t)} \right\}. \tag{3.4}$$

An alternative to $\Lambda_h(t)$ defined by (3.4) is as follows: let $\{\mathbf{x}_i\}_{i=1}^{N_B}$ be a set of points from $\overline{B(t)}$ which cover $\overline{B(t)}$ (uniformly, for example); we define then

$$\Lambda_h(t) = \left\{ \boldsymbol{\mu}_h \mid \boldsymbol{\mu}_h = \sum_{i=1}^{N_B} \boldsymbol{\mu}_i \delta(\mathbf{x} - \mathbf{x}_i),\ \boldsymbol{\mu}_i \in \mathbb{R}^2\ \forall i = 1, \ldots N_B \right\}, \tag{3.5}$$

where $\delta(\cdot)$ is the *Dirac measure* at $\mathbf{x} = 0$. Then instead of the scalar product of $(H^1(B_h(t)))^2$ we shall use $\langle \cdot, \cdot \rangle_{\Lambda_h(t)}$ defined by

$$\langle \boldsymbol{\mu}_h, \mathbf{v}_h \rangle_{\Lambda_h(t)} = \sum_{i=1}^{N_B} \boldsymbol{\mu}_i \cdot \mathbf{v}_h(\mathbf{x}_i) \quad \forall \boldsymbol{\mu}_h \in \Lambda_h(t),\ \ \mathbf{v}_h \in W_{\mathbf{g}_{0h}} \text{ or } W_{0h}. \tag{3.6}$$

The approach, based on (3.5) and (3.6), makes little sense for the continuous problem, but is meaningful for the discrete problem; it amounts to forcing the rigid body motion of $B(t)$ via a *collocation method*. A similar technique has been used to enforce Dirichlet boundary conditions by Bertrand et al. (Ref. [17]).

Remark 3.1. *The bilinear form in* (3.6) *has definitely the flavor of a discrete* $L^2(B(t))$*-scalar product. Let us insist on the fact that taking* $\Lambda(t) = (L^2(\Omega))^d$*, and then*

$$(\boldsymbol{\mu}, \mathbf{v})_{\Lambda(t)} = \int_\Omega \boldsymbol{\mu} \cdot \mathbf{v}\, d\mathbf{x} \quad \forall \boldsymbol{\mu} \text{ and } \mathbf{v} \in \Lambda(t),$$

makes no sense for the continuous problem. On the other hand, it makes sense for the discrete problem in (2.43)–(2.48)*, but do not expect* $\boldsymbol{\lambda}_h(t)$ *to converge to a* L^2*-function as* $h \to 0$ *(it will converge to some element of* $(H^1(B(t))')^2$*, where* $H^1(B(t))'$ *is the dual space of* $H^1(B(t))$*).*

Using the above finite dimensional spaces leads to the following approximation of problems (2.43)–(2.49):

For $t > 0$ find $\{\mathbf{u}_h(t), p_h(t), \mathbf{V}_\mathbf{G}(t), \mathbf{G}(t), \omega(t), \boldsymbol{\lambda}_h(t)\}$ such that

$$\mathbf{u}_h(t) \in W_{\mathbf{g}_{0h}(t)},\ \ p_h(t) \in L^2_{0h},\ \ \mathbf{V}_\mathbf{G}(t) \in \mathbb{R}^2,\ \ \mathbf{G}(t) \in \mathbb{R}^2,\ \ \omega(t) \in \mathbb{R},\ \ \boldsymbol{\lambda}_h(t) \in \Lambda_h(t) \tag{3.7}$$

and

$$\begin{aligned}
&\rho_\mathrm{f} \int_\Omega \frac{\partial \mathbf{u}_h}{\partial t} \cdot \mathbf{v}\, \mathrm{d}\mathbf{x} + \rho_\mathrm{f} \int_\Omega (\mathbf{u}_h \cdot \nabla)\mathbf{u}_h \cdot \mathbf{v}\, \mathrm{d}x - \int_\Omega p_h \nabla \cdot \mathbf{v}\, \mathrm{d}\mathbf{x} + 2\nu_\mathrm{f} \int_\Omega \mathbf{D}(\mathbf{u}_h) : \mathbf{D}(\mathbf{v})\, \mathrm{d}\mathbf{x} \\
&\quad + (1 - \rho_\mathrm{f}/\rho_\mathrm{s}) M \frac{\mathrm{d}\mathbf{V}_\mathbf{G}}{\mathrm{d}t} \cdot \mathbf{Y} + (1 - \rho_\mathrm{f}/\rho_\mathrm{s}) \mathbf{I} \frac{\mathrm{d}\omega}{\mathrm{d}t} \theta - \mathbf{F}^r \cdot \mathbf{Y} - (\boldsymbol{\lambda}_h, \mathbf{v} - \mathbf{Y} - \boldsymbol{\theta} \times \mathbf{G}\mathbf{x})_{\Lambda_h(t)} \\
&\qquad = (1 - \rho_\mathrm{f}/\rho_\mathrm{s}) M \mathbf{g} \cdot \mathbf{Y} + \rho_\mathrm{f} \int_\Omega \mathbf{g} \cdot \mathbf{v}\, \mathrm{d}\mathbf{x} \quad \forall \mathbf{v} \in W_{0h}, \mathbf{Y} \in \mathbb{R}^2, \theta \in \mathbb{R},
\end{aligned} \tag{3.8}$$

$$\int_\Omega q \nabla \cdot \mathbf{u}_h(t)\, \mathrm{d}x = 0 \quad \forall q \in L^2_h, \tag{3.9}$$

$$\frac{\mathrm{d}\mathbf{G}}{\mathrm{d}t} = \mathbf{V}_\mathbf{G}, \tag{3.10}$$

$$(\boldsymbol{\mu}_h, \mathbf{u}_h(t) - \mathbf{V}_\mathbf{G}(t) - \boldsymbol{\omega}(t) \times \mathbf{G}(t)\mathbf{x})_{\Lambda_h(t)} = 0 \quad \forall \boldsymbol{\mu}_h \in \Lambda_h(t), \tag{3.11}$$

$$\mathbf{V}_\mathbf{G}(0) = \mathbf{V}^0, \quad \omega(0) = \omega^0, \quad \mathbf{G}(0) = \mathbf{G}^0; \tag{3.12}$$

$$\mathbf{u}_h(\mathbf{x}, 0) = \mathbf{u}_{0h}(\mathbf{x}) \quad \forall \mathbf{x} \in \Omega \setminus \overline{B_h(0)}, \qquad \mathbf{u}_h(\mathbf{x}, 0) = \mathbf{V}^0 + \boldsymbol{\omega}^0 \times \mathbf{G}^0\mathbf{x} \quad \forall \mathbf{x} \in \overline{B_h(0)}. \tag{3.13}$$

Remark 3.2. *In relation* (3.8), *we can replace* $2\int_\Omega \mathbf{D}(\mathbf{u}_h) : \mathbf{D}(\mathbf{v})\mathrm{d}\mathbf{x}$ *by* $\int_\Omega \nabla \mathbf{u}_h : \nabla \mathbf{v}\, \mathrm{d}\mathbf{x}$, *by taking Remark* 2.4 *into account*.

Remark 3.3. *Let* h_Ω (*resp*., $h_{B(t)}$) *be the mesh size of a regular triangulation of* $\bar{\Omega}$ (*resp*., $\bar{B}(t)$) *then* $h_\Omega < \kappa h_{B(t)} < h_{B(t)} < 2h_\Omega$ *for* $\kappa < 1$ *is needed in order to satisfy some kind of stability condition* (*for generalities on the approximation of mixed variational problems*, *such as* (3.7)–(3.13), *involving Lagrange multipliers*, *see*, *for example*, *the publications by Brezzi and Fortin* (*Ref*. [18]) *and Roberts and Thomas* (*Ref*. [19]).

Remark 3.4. *In order to avoid the solution at each time step of complicated triangulation intersection problems we advocate the use of*

$$(\boldsymbol{\lambda}_h, \pi_h \mathbf{v} - \mathbf{Y} - \boldsymbol{\theta} \times \mathbf{G}(t)\mathbf{x})_{\Lambda_h(t)} \tag{3.14}$$

resp.,

$$\Big(\boldsymbol{\mu}_h, \pi_h \mathbf{u}_h(t) - \mathbf{V}_\mathbf{G}(t) - \boldsymbol{\omega}(t) \times \mathbf{G}(t)\mathbf{x})_{\Lambda_h(t)}\Big) \tag{3.15}$$

in (3.8) (*resp*., (3.11)), *instead of*

$$(\boldsymbol{\lambda}_h, \mathbf{v} - \mathbf{Y} - \boldsymbol{\theta} \times \mathbf{G}(t)\mathbf{x})_{\Lambda_h(t)}$$

resp.,

$$\Big(\boldsymbol{\mu}_h, \mathbf{u}_h(t) - \mathbf{V}_\mathbf{G}(t) - \boldsymbol{\omega}(t) \times \mathbf{G}(t)\mathbf{x})_{\Lambda_h(t)}\Big),$$

where, *in* (3.14) *and* (3.15), $\pi_h : (C^0(\bar{\Omega}))^2 \to \Lambda_h(t)$ *is the* piecewise linear interpolation *operator*, *which*, *to each function* $\mathbf{w}$ *belonging to* $(C^0(\bar{\Omega}))^2$ *associates the unique element of* $\Lambda_h(t)$ *defined from the values taken by* $\mathbf{w}$ *at the vertices of* $\mathcal{T}_{B_h(t)}$.

Remark 3.5. *If B is either a disk or a spherical ball, we can take advantage of the rotational invariance of B and, for $t \geqslant 0$, derive $\tau_{B_h(t)}$ from $\tau_{B_h(0)}$ by translation. If B is not rotationally invariant, we shall take $\mathscr{T}_{B_h(t)}$ rigidly attached to B.*

Remark 3.6. *In general, the function $\mathbf{u}(t)$ has no more than the $(H^{3/2}(\Omega))^2$-regularity. This low regularity implies that we cannot expect more than $\mathrm{O}(h^{3/2})$ for the approximation error $\|\mathbf{u}_h(t) - \mathbf{u}(t)\|_{L^2(\Omega)}$.*

4. Time discretization by operator splitting

4.1. Generalities

Following Chorin (Refs. [20–22]), most 'modern' Navier–Stokes solvers are based on operator splitting algorithms (see, e.g., Refs. [23,24]) in order to force the incompressibility condition via a Stokes solver or a L^2-projection method. This approach still applies to the initial value problem (3.7)–(3.13) which contains four numerical difficulties to each of which can be associated a specific operator, namely

(a) The incompressibility condition and the related unknown pressure.
(b) An advection–diffusion term.
(c) The rigid body motion of $B_h(t)$ and the related multiplier $\boldsymbol{\lambda}_h(t)$.
(d) The collision term $\mathbf{F}^r$.

The operators in (a) and (c) are essentially *projection operators*. From an abstract point of view, problem (3.7)–(3.13) is a particular case of the following class of initial value problems

$$\frac{\mathrm{d}\varphi}{\mathrm{d}t} + A_1(\varphi, t) + A_2(\varphi, t) + A_3(\varphi, t) + A_4(\varphi, t) = f, \quad \varphi(0) = \varphi_0, \tag{4.1}$$

where the operators A_i can be *multivalued*. Among the many operator-splitting methods which can be employed to solve (4.1), we advocate (following, e.g., [25]) the very simple one below; it is only first order accurate, but its low order accuracy is compensated by good stability and robustness properties. Actually, this scheme can be made second order accurate by *symmetrization* (see, e.g., [26,27] for the application of *symmetrized* splitting schemes to the solution of the Navier–Stokes equations).

A fractional step scheme á la Marchuk–Yanenko: With $\Delta t(> 0)$ a *time discretization step*, applying the *Marchuk–Yanenko scheme* to the initial value problem (4.1) leads to

$$\varphi^0 = \varphi_0 \tag{4.2}$$

and for $n \geqslant 0$, compute φ^{n+1} from φ^n via

$$\frac{\varphi^{n+j/4} - \varphi^{n+(j-1)/4}}{\Delta t} + A_j(\varphi^{n+j/4}, (n+1)\Delta t) = f_j^{n+1}, \tag{4.3}$$

for $j = 1, 2, 3, 4$ with $\sum_{j=1}^4 f_j^{n+1} = f^{n+1}$.

4.2. Application of the Marchuk–Yanenko scheme to particulate flow

Applying scheme (4.2) and (4.3) to problem (3.7)–(3.13), we obtain (with $0 \leqslant \alpha,\ \beta \leqslant 1,\ \alpha + \beta = 1$ and after dropping some of the subscripts h and denoting $\mathbf{V}_{\mathbf{G}^n}$ by $\mathbf{V}^n$):

$$\mathbf{u}^0 = \mathbf{u}_{0h},\ \mathbf{V}^0, \omega^0 \text{ and } \mathbf{G}^0 \text{ are given}, \tag{4.4}$$

for $n \geqslant 0$, knowing $\mathbf{u}^n, \mathbf{V}^n, \omega^n, \mathbf{G}^n$, we compute $\mathbf{u}^{n+1/4},\ p^{n+1/4}$ via the solution of

$$\begin{aligned} &\rho_{\mathrm{f}} \int_\Omega \frac{\mathbf{u}^{n+1/4} - \mathbf{u}^n}{\Delta t} \cdot \mathbf{v}\, \mathrm{d}\mathbf{x} - \int_\Omega p^{n+1/4} \nabla \cdot \mathbf{v}\, \mathrm{d}\mathbf{x} = 0 \quad \forall \mathbf{v} \in W_{0h}, \\ &\int_\Omega q \nabla \cdot \mathbf{u}^{n+1/4}\, \mathrm{d}\mathbf{x} = 0 \quad \forall q \in L_h^2;\ \mathbf{u}^{n+1/4} \in W_{\mathbf{g}_{0h}}^{n+1},\ p^{n+1/4} \in L_{0h}^2. \end{aligned} \tag{4.5}$$

Next we compute $\mathbf{u}^{n+2/4}$ via the solution of

$$\rho_f \int_\Omega \frac{\mathbf{u}^{n+2/4}-\mathbf{u}^{n+1/4}}{\Delta t}\cdot\mathbf{v}\,d\mathbf{x} + 2\alpha\nu_f\int_\Omega \mathbf{D}(\mathbf{u}^{n+2/4}):\mathbf{D}(\mathbf{v})\,d\mathbf{x} + \rho_f\int_\Omega(\mathbf{u}^{n+1/4}\cdot\nabla)\mathbf{u}^{n+2/4}\cdot\mathbf{v}\,d\mathbf{x}$$
$$= \rho_f\int_\Omega \mathbf{g}\cdot\mathbf{v}\,d\mathbf{x}\quad \forall\mathbf{v}\in W_{0h};\ \mathbf{u}^{n+2/4}\in W_{\mathbf{g}_{0h}}^{n+1}, \tag{4.6}$$

and then, predict the position and the translation velocity of the center of mass as follows:

Take $\mathbf{V}^{n+3/4,0}=\mathbf{V}^n$ and $\mathbf{G}^{n+3/4,0}=\mathbf{G}^n$; then predict the new position and translation velocity of B_h via the following subcycling technique:

For $k=1,\dots,N$, compute

$$\widehat{\mathbf{V}}^{n+3/4,k}=\mathbf{V}^{n+3/4,k-1}+(\Delta t/N)(\mathbf{g}+(1-\rho_f/\rho_s)^{-1}M^{-1}\mathbf{F}^r(\mathbf{G}^{n+3/4,k-1})), \tag{4.7a}$$

$$\widehat{\mathbf{G}}^{n+3/4,k}=\mathbf{G}^{n+3/4,k-1}+(\Delta t/2N)(\widehat{\mathbf{V}}^{n+3/4,k}+\mathbf{V}^{n+3/4,k-1}), \tag{4.7b}$$

$$\mathbf{V}^{n+3/4,k}=\mathbf{V}^{n+3/4,k-1}+(\Delta t/N)\mathbf{g}+(\Delta t/2N)(1-\rho_f/\rho_s)^{-1}M^{-1}(\mathbf{F}^r(\widehat{\mathbf{G}}^{n+3/4,k})+\mathbf{F}^r(\mathbf{G}^{n+3/4,k-1})), \tag{4.7c}$$

$$\mathbf{G}^{n+3/4,k}=\mathbf{G}^{n+3/4,k-1}+(\mathbf{V}^{n+3/4,k}+\mathbf{V}^{n+3/4,k-1})(\Delta t/2N), \tag{4.7d}$$

enddo;

and let $\mathbf{V}^{n+3/4}=\mathbf{V}^{n+3/4,N}$, $\mathbf{G}^{n+3/4}=\mathbf{G}^{n+3/4,N}$.

Finally, we compute $\mathbf{u}^{n+1}$, $\boldsymbol{\lambda}^{n+1}$, $\mathbf{V}^{n+1},\omega^{n+1}$ via the solution of

$$\rho_f\int_\Omega\frac{\mathbf{u}^{n+1}-\mathbf{u}^{n+2/4}}{\Delta t}\cdot\mathbf{v}\,d\mathbf{x}+2\beta\nu_f\int_\Omega\mathbf{D}(\mathbf{u}^{n+1}):\mathbf{D}(\mathbf{v})\,d\mathbf{x}$$
$$+(1-\rho_f/\rho_s)\mathbf{I}\frac{\omega^{n+1}-\omega^n}{\Delta t}\theta+(1-\rho_f/\rho_s)M\frac{\mathbf{V}^{n+1}-\mathbf{V}^{n+3/4}}{\Delta t}\cdot\mathbf{Y}$$
$$=(\boldsymbol{\lambda}^{n+1},\mathbf{v}-\mathbf{Y}-\boldsymbol{\theta}\times\mathbf{G}^{n+3/4}\mathbf{x})_{B_h^{n+3/4}}\quad\forall\mathbf{v}\in W_{0h},\mathbf{Y}\in\mathbb{R}^2,\theta\in\mathbb{R}, \tag{4.8a}$$

$$(\boldsymbol{\mu},\mathbf{u}^{n+1}-\mathbf{V}^{n+1}-\boldsymbol{\omega}^{n+1}\times\mathbf{G}^{n+3/4}\mathbf{x})_{B_h^{n+3/4}}=0\quad\forall\boldsymbol{\mu}\in\Lambda_h^{n+3/4}; \tag{4.8b}$$

$$\mathbf{u}^{n+1}\in W_{\mathbf{g}_{0h}}^{n+1},\quad \boldsymbol{\lambda}^{n+1}\in\Lambda_h^{n+3/4}; \tag{4.8c}$$

then take $\mathbf{G}^{n+1,0}=\mathbf{G}^{n+3/4}$; then correct the position of the rigid body center as follows:

For $k=1,\dots,N$, compute

$$\widehat{\mathbf{G}}^{n+1,k}=\mathbf{G}^{n+1,k-1}+(\Delta t/2N)(\mathbf{V}^n+\mathbf{V}^{n+1}), \tag{4.9a}$$

$$\mathbf{G}^{n+1,k}=\widehat{\mathbf{G}}^{n+1,k}+\frac{(\Delta t)^2}{4N^2}(1-\rho_f/\rho_s)^{-1}M^{-1}(\mathbf{F}^r(\widehat{\mathbf{G}}^{n+1,k})+\mathbf{F}^r(\mathbf{G}^{n+1,k-1})), \tag{4.9b}$$

enddo;

and let $\mathbf{G}^{n+1}=\mathbf{G}^{n+1,N}$.

In (4.4)–(4.9b) we have $W_{\mathbf{g}_{0h}}^{n+1}=W_{\mathbf{g}_0}((n+1)\Delta t)h$, $\Lambda_h^s=\Lambda_h(s\Delta t)$, and $B_h^s=B_h(s\Delta t)$. Using operator splitting, we can use time steps much smaller than Δt to predict and correct, as in (4.7a)–(4.7d) and (4.9a) and (4.9b), the position of the center of mass, without changing the time step Δt in algorithm (4.4)–(4.9). For our numerical simulations, we have used $\alpha=1$ and $\beta=0$ in (4.6) and (4.8a)–(4.8c) and $N=10$ in (4.7a)–(4.7d) and (4.9a) and (4.9b).

4.3. Solution of the subproblem (4.5)

By inspection of (4.5) it is clear that $\mathbf{u}^{n+1/4}$ is the $(L^2(\Omega))^2$-projection of $\mathbf{u}^n$ on the (affine) subset of the functions $\mathbf{v} \in W^{n+1}_{\mathbf{g}_{0h}}$ such that $\int_\Omega q\nabla\cdot\mathbf{v}\,d\mathbf{x} = 0\ \forall q \in L^2_h$, and that $p^{n+1/4}$ is the corresponding Lagrange multiplier in L^2_{0h}. The pair $\{\mathbf{u}^{n+1/4},\ p^{n+1/4}\}$ is *unique* and to compute it we can use an *Uzawa/conjugate gradient* algorithm operating in L^2_{0h} equipped with the scalar product $\{q, q'\} \to \int_\Omega \nabla q\cdot\nabla q'\,d\mathbf{x}$. We obtained then an algorithm preconditioned by the discrete equivalent of $-\Delta$ for the homogeneous Neumann boundary condition. It follows from, e.g., [6], that such an algorithm, applied to the solution of

$$\rho_f\int_\Omega \frac{\mathbf{u}-\mathbf{u}^*}{\Delta t}\cdot\mathbf{v}\,d\mathbf{x} - \int_\Omega p\nabla\cdot\mathbf{v}\,d\mathbf{x} = 0 \quad \forall\mathbf{v}\in W_{0h},$$
$$\int_\Omega q\nabla\cdot\mathbf{u}\,d\mathbf{x} = 0 \quad \forall q\in L^2_h;\ \mathbf{u}\in W^{n+1}_{\mathbf{g}_{0h}},\ \ p\in L^2_{0h}, \tag{4.10}$$

reads as follows:

$$p_0 \text{ is given in } L^2_{0h}; \tag{4.11}$$

solve

$$\mathbf{u}_0 \in W^{n+1}_{\mathbf{g}_{0h}},$$
$$\rho_f\int_\Omega \mathbf{u}_0\cdot\mathbf{v}\,d\mathbf{x} = \rho_f\int_\Omega \mathbf{u}^*\cdot\mathbf{v}\,d\mathbf{x} + \nabla t\int_\Omega p_0\nabla\cdot\mathbf{v}\,d\mathbf{x} \quad \forall\mathbf{v}\in W_{0h}, \tag{4.12}$$

$$g_0 \in L^2_{0h},$$
$$\int_\Omega \nabla g_0\cdot\nabla q\,d\mathbf{x} = \int_\Omega \nabla\cdot\mathbf{u}_0\,d\mathbf{x} \quad \forall q\in L^2_h, \tag{4.13}$$

and set

$$w^0 = g^0. \tag{4.14}$$

Then for $k \geqslant 0$, assuming that p_k, g_k, w_k are known, we compute p_{k+1}, g_{k+1} and, if necessary w_{k+1} as follows:
solve:

$$\bar{\mathbf{u}}_k \in W_{0h},$$
$$\rho_f\int_\Omega \bar{\mathbf{u}}_k\cdot\mathbf{v}\,d\mathbf{x} = \Delta t\int_\Omega w_k\nabla\cdot\mathbf{v}\,d\mathbf{x} \quad \forall\mathbf{v}\in W_{0h}, \tag{4.15}$$

$$\bar{g}_k \in L^2_{0h},$$
$$\int_\Omega \nabla\bar{g}_k\cdot\nabla q\,d\mathbf{x} = \int_\Omega \nabla\cdot\bar{\mathbf{u}}_k q\,d\mathbf{x} \quad \forall q\in L^2_h, \tag{4.16}$$

and compute

$$\rho_k = \int_\Omega |\nabla g_k|^2\,d\mathbf{x}\Big/\int_\Omega \nabla\cdot\bar{\mathbf{u}}_k w_k\,d\mathbf{x}, \tag{4.17}$$

$$p_{k+1} = p_k - \rho_k w_k, \tag{4.18}$$
$$g_{k+1} = g_k - \rho_k\bar{g}_k. \tag{4.19}$$

If $\int_\Omega |\nabla g_{k+1}|^2\,d\mathbf{x}/\int_\Omega |\nabla g_0|^2\,d\mathbf{x} \leqslant \epsilon$, take $p = p_{k+1}$; else compute

$$\gamma_k = \int_\Omega |\nabla g_{k+1}|^2\,d\mathbf{x}\Big/\int_\Omega |\nabla g_k|^2\,d\mathbf{x} \tag{4.20}$$

and set

$$w_{k+1} = g_{k+1} + \gamma_k w_k. \tag{4.21}$$

Do $k = k + 1$ and go back to (4.15).

Algorithms (4.11)–(4.21) is very easy to implement and has very good convergence properties.

4.4. Solution of the subproblems (4.6)

If $\alpha > 0$, problem (4.6) is a *linear advection–diffusion* problem; it can be easily solved by a least squares/conjugate gradient algorithm, like those discussed in, e.g., ch. 7 of Ref. [28].

4.5. Solution of the subproblems (4.8a)–(4.8c)

The solution of problems (4.8a)–(4.8c) can be computed by algorithms similar to those in [1] for elliptic problems, with the additional difficulty that there are here three more equations, namely the ones used to compute the translation velocity and angular speed of the rigid body. Problem (4.8a)–(4.8c) has the following form:

$$\begin{aligned}&\rho_{\mathrm{f}} \int_\Omega \frac{\mathbf{u} - \mathbf{u}\,*}{\Delta t} \cdot \mathbf{v}\, \mathrm{d}\mathbf{x} + 2\beta\nu_{\mathrm{f}} \int_\Omega \mathbf{D}(\mathbf{u}) : \mathbf{D}(\mathbf{v})\, \mathrm{d}\mathbf{x} \\ &\quad + (1 - \rho_{\mathrm{f}}/\rho_{\mathrm{s}}) I \frac{\omega - \omega^*}{\Delta t}\theta + (1 - \rho_{\mathrm{f}}/\rho_{\mathrm{s}}) M \frac{\mathbf{V} - \mathbf{V}^*}{\Delta t} \cdot \mathbf{Y}\end{aligned} \tag{4.22}$$

$$-(\boldsymbol{\lambda}, \mathbf{v} - \mathbf{Y} - \theta \times \mathbf{G}\mathbf{x})_{B_h} = 0 \quad \forall \mathbf{v} \in W_{0h},\ \ \mathbf{Y} \in \mathbb{R}^2,\ \ \theta \in \mathbb{R},$$

$$(\boldsymbol{\mu}, \mathbf{u} - \mathbf{V} - \boldsymbol{\omega} \times \mathbf{G}\mathbf{x})_{B_h} = 0 \quad \forall \boldsymbol{\mu} \in \Lambda_h;\ \ \mathbf{u} \in W_{\mathbf{g}_{0h}},\ \ \boldsymbol{\lambda} \in \Lambda_h, \tag{4.23}$$

where the center of mass $\mathbf{G}$ of the rigid body B_h is known and where $W_{\mathbf{g}_{0h}} = W^{n+1}_{\mathbf{g}_{oh}}$.

Problem (4.22) and (4.23) is itself a particular case of the following saddle-point system

$$\mathbf{A}\mathbf{x} + \mathbf{B}^t\mathbf{y} = \mathbf{b}, \quad \mathbf{B}\mathbf{x} = \mathbf{c}, \tag{4.24}$$

where $\mathbf{A}$ is symmetric and positive definite if $\rho_{\mathrm{s}} > \rho_{\mathrm{f}}$. It follows from e.g., [29] and [30], that problem (4.24) can be solved by Uzawa/conjugate gradient algorithms. Applying such an algorithm to problem (4.22), (4.23) leads to

$$\boldsymbol{\lambda}^0 \text{ is given in } \Lambda_h, \tag{4.25}$$

solve

$$\rho_{\mathrm{f}} \int_\Omega \mathbf{u}^0 \cdot \mathbf{v}\, \mathrm{d}\mathbf{x} + 2\Delta t\beta\nu_{\mathrm{f}} \int_\Omega \mathbf{D}(\mathbf{u}^0) : \mathbf{D}(\mathbf{v})\, \mathrm{d}\mathbf{x} = \rho_{\mathrm{f}} \int_\Omega \mathbf{u}^* \cdot \mathbf{v}\, \mathrm{d}\mathbf{x} + \Delta t(\boldsymbol{\lambda}^0, \mathbf{v})_{B_h} \quad \forall \mathbf{v} \in W_{0h};\ \ \mathbf{u}^0 \in W_{\mathbf{g}_{0h}}, \tag{4.26}$$

$$(1 - \rho_{\mathrm{f}}/\rho_{\mathrm{s}}) M\mathbf{V}^0 \cdot \mathbf{Y} = (1 - \rho_{\mathrm{f}}/\rho_{\mathrm{s}}) M\mathbf{V}^* \cdot \mathbf{Y} - \Delta t(\boldsymbol{\lambda}^0, \mathbf{Y})_{B_h} \quad \forall \mathbf{Y} \in \mathbb{R}^2;\ \ \mathbf{V}^0 \in \mathbb{R}^2, \tag{4.27}$$

$$(1 - \rho_{\mathrm{f}}/\rho_{\mathrm{s}}) I\omega^0\theta = (1 - \rho_{\mathrm{f}}/\rho_{\mathrm{s}}) I\omega^*\theta - \Delta t(\boldsymbol{\lambda}^0, \theta \times \mathbf{G}\mathbf{x})_{B_h} \quad \forall \theta \in \mathbb{R};\ \ \omega^0 \in \mathbb{R}, \tag{4.28}$$

then

$$(\boldsymbol{\mu}, \mathbf{g}^0)_{B_h} = (\boldsymbol{\mu}, \mathbf{u}^0 - \mathbf{V}^0 - \omega^0 \times \mathbf{G}\mathbf{x})_{B_h} \quad \forall \boldsymbol{\mu} \in \Lambda_h;\ \ \mathbf{g}^0 \in \Lambda_h, \tag{4.29}$$

and set

$$\mathbf{w}^0 = \mathbf{g}^0. \tag{4.30}$$

Then, for $k \geqslant 0$, assuming that $\boldsymbol{\lambda}^k$, $\mathbf{g}^k$, $\mathbf{w}^k$, $\mathbf{u}^k$, $\mathbf{V}^k$, ω^k are known, we obtain $\boldsymbol{\lambda}^{k+1}$, $\mathbf{g}^{k+1}$, $\mathbf{w}^{k+1}\mathbf{u}^{k+1}$, $\mathbf{V}^{k+1}$, ω_p^{k+1} as follows:

solve

$$\rho_f \int_\Omega \bar{\mathbf{u}}^k \cdot \mathbf{v}\, d\mathbf{x} + 2\Delta t \beta \nu_f \int_\Omega \mathbf{D}(\bar{\mathbf{u}}^k) : \mathbf{D}(\mathbf{v}) d\mathbf{x} = \Delta t (\mathbf{w}^k, \mathbf{v})_{B_h} \quad \forall \mathbf{v} \in W_{0h};\ \ \bar{\mathbf{u}}^k \in W_{0h}, \tag{4.31}$$

$$(1 - \rho_f/\rho_s) M \bar{\mathbf{V}}^k \cdot \mathbf{Y} = -\Delta t (\mathbf{w}^k, \mathbf{Y})_{B_h} \quad \forall \mathbf{Y} \in \mathbb{R}^2;\ \ \bar{\mathbf{V}}^k \in \mathbb{R}^2, \tag{4.32}$$

$$(1 - \rho_f/\rho_s) I \bar{\omega}^k \theta = -\Delta t (\mathbf{w}^k, \boldsymbol{\theta} \times \mathbf{G}\mathbf{x})_{B_h} \quad \forall \theta \in \mathbb{R};\ \ \bar{\omega}^k \in \mathbb{R}, \tag{4.33}$$

and then

$$(\boldsymbol{\mu}, \bar{\mathbf{g}}^k)_{B_h} = \left(\boldsymbol{\mu}, \bar{\mathbf{u}}^k - \bar{\mathbf{V}}^k - \bar{\omega}^k \times \mathbf{G}\mathbf{x}\right)_{B_h} \quad \forall \boldsymbol{\mu} \in \Lambda_h;\ \ \bar{\mathbf{g}}^k \in \Lambda_h. \tag{4.34}$$

Compute

$$\rho_k = (\mathbf{g}^k, \mathbf{g}^k)_{B_h} \Big/ (\mathbf{w}^k, \bar{\mathbf{g}}^k)_{B_h}, \tag{4.35}$$

and then

$$\boldsymbol{\lambda}^{k+1} = \boldsymbol{\lambda}^k - \rho_k \mathbf{w}^k, \tag{4.36}$$

$$\mathbf{u}^{k+1} = \mathbf{u}^k - \rho_k \bar{\mathbf{u}}^k, \tag{4.37}$$

$$\mathbf{V}^{k+1} = \mathbf{V}^k - \rho_k \bar{V}^k, \tag{4.38}$$

$$\omega^{k+1} = \omega^k - \rho_k \bar{\omega}^k, \tag{4.39}$$

$$\mathbf{g}^{k+1} = \mathbf{g}^k - \rho_k \bar{\mathbf{g}}^k. \tag{4.40}$$

If $(\mathbf{g}^{k+1}, \mathbf{g}^{k+1})_{B_h} / (\mathbf{g}^0, \mathbf{g}^0)_{B_h} \leqslant \epsilon$, take $\mathbf{u} = \mathbf{u}^{k+1},\ \mathbf{V} = \mathbf{V}^{k+1}$ and $\omega = \omega^{k+1}$. Else, compute

$$\gamma_k = (\mathbf{g}^{k+1}, \mathbf{g}^{k+1})_{B_h} / (\mathbf{g}^k, \mathbf{g}^k)_{B_h}, \tag{4.41}$$

and set

$$\mathbf{w}^{k+1} = \mathbf{g}^{k+1} + \gamma_k \mathbf{w}^k. \tag{4.42}$$

Do $k = k + 1$ and go back to (4.31).

Remark 4.1. *If* $\rho_s \leqslant \rho_f$, *the corresponding matrix* $\mathbf{A}$ *in* (4.24) *is no longer positive definite. However, due to the small dimension of* $\{\mathbf{V}, \omega\}$, *it is very easy to adapt algorithm* (4.25)–(4.41) *to the case* $\rho_s \leqslant \rho_f$. *Similarly, there is no practical difficulty at treating the neutrally buoyant case* $(\rho_s = \rho_f)$.

5. Remarks on the computational treatment of particle collisions

In the above sections, we have considered the particular case of a *single particle* moving in a region Ω filled with a Newtonian incompressible viscous fluid; we took into account possible particle-boundary collisions via the repulsion force $\mathbf{F}^r$, but we did not provide, yet, an explicit form of $\mathbf{F}^r$. Actually, the above methodology can be generalized fairly easily to *many particles* cases, with however, a computational difficulty: one has to prevent particle interpenetration or particle/boundary penetration. To achieve those goals we have included in the *Newton–Euler equations* modeling particle motions a *short range repulsing force*. If we consider the particular case of circular particles (in 2-D) or *spherical* particles in (3-D), and if B_i and B_j are such two particles, with radius R_i and R_j and centers of mass $\mathbf{G}_i$ and $\mathbf{G}_j$, we shall require the repulsion force $\vec{F}_{ij}$ between B_i and B_j to satisfy the following properties:

(i) To be parallel to $\overrightarrow{\mathbf{G}_i\mathbf{G}_j}$.

(ii) To verify

$$|\vec{F}_{ij}| = 0 \text{ if } d_{ij} \geqslant R_i + R_j + \rho, \quad |\vec{F}_{ij}| = c/\varepsilon \text{ if } d_{ij} = R_i + R_j \tag{5.1}$$

with $d_{ij} = |\overrightarrow{\mathbf{G}_i\mathbf{G}_j}|$, c a *scaling factor* and ε a '*small*' *positive number*.

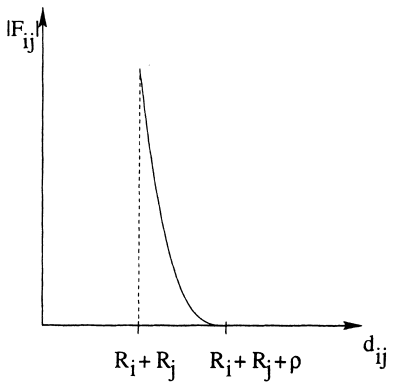

Fig. 4. Repulsion force behavior.

(iii) $|\vec{F}_{ij}|$ has behave as in Fig. 4, for

$$R_i + R_j \leqslant d_{ij} \leqslant R_i + R_j + \rho.$$

Parameter ρ is the *range* of the repulsion force; for the simulations discussed in the following section we have taken $\rho \simeq h_\Omega$. Boundary/particle collisions can be treated in a similar way (see [13] for details).

Remark 5.1. *The above collision model is fairly simple and is inspired from penalty techniques classically used for the computational treatment of some contact problems in Mechanics* (*see*, *e.g.*, [30,31] *for details and applications*). *Despite its simplicity*, *this model produces good results*, *the main reason for that being*, *in our opinion*, *that if the fluid is sufficiently viscous and if the fluid and particle densities are close*, *the collisions – if they occur – are nonviolent ones*, *implying that the particles which are going to collide move at almost the same velocity just before collision*. *For more sophisticated models allowing more violent collisions see*, *e.g.*, [14] *and the references therein*.

Remark 5.2. *For those readers wondering how* h, ρ, *and* c/ϵ *are adjusted we would like to do the following comments*: *clearly the space discretization parameter* h *is adjusted so that the finite element approximation can resolve the boundary and shear layers occurring in the flow*. *Next*, *it is clear that* ρ *can be taken of the order of* h. *The choice of* c/ϵ *is more subtle*; *let us say that simple model problems for harmonic oscillators with rigid obstacles* (*see Ref.* [32] *for details*) *show that we can expect interpenatration of the order of* $\sqrt{\epsilon/c}$; *this suggests therefore to take* $\rho \gg \sqrt{\epsilon/c}$, *which is what we did in our calculations*.

6. Numerical experiments

We are going to present now the results of numerical experiments for 2-D and 3-D flow.

6.1. Flow around a NACA0012 airfoil which has a fixed center and is free to rotate due to hydrodynamical forces

Here we consider an incompressible viscous flow around a NACA0012 airfoil which has a fixed center of mass and is free to rotate due to hydrodynamical forces; the surrounding region Ω is the rectangle $(-4, 16) \times (-2, 2)$. The characteristic length, namely the airfoil length, is 1.008930411365 and the fixed center of mass of the NACA0012 airfoil is at (0.420516, 0). Initial angular velocity and incident angle are zeroes. The density of the fluid $\rho_f = 1.0$ and the density of the airfoil $\rho_s = 1.1$. The viscosity of the fluid is $\nu_f = 0.00125$. The initial condition for the fluid flow is $\mathbf{u} = \mathbf{0}$ and the boundary data $\mathbf{g}_0$ is given by

$$\mathbf{g}_0(\mathbf{x},t)=\begin{cases}\mathbf{0} & \text{if } x_2=-2 \text{ or } 2,\\ (1-e^{-50t})\begin{pmatrix}1\\0\end{pmatrix} & \text{if } x_1=-4 \text{ or } 16,\end{cases}$$

for $t \geqslant 0$, but we could have used another function $\mathbf{g}_0$. Hence the Reynolds number is about 807 with respect to the characteristic length of the NACA0012 airfoil and the maximal inflow speed. The time step is varied from $\Delta t = 0.001$ to about 0.0005. The mesh size for the velocity field is $h_v = 1/96$ (there are 739,585 nodes). The mesh size for pressure is $h_p = 1/48$ (185,473 nodes). In this test case, the mesh size $h_v = 1/96$ is required to catch the velocity field close to the leading edge of the NACA0012 airfoil. For the airfoil mesh necessary at each time step, we have just chosen all the grid points from the velocity grid contained in the

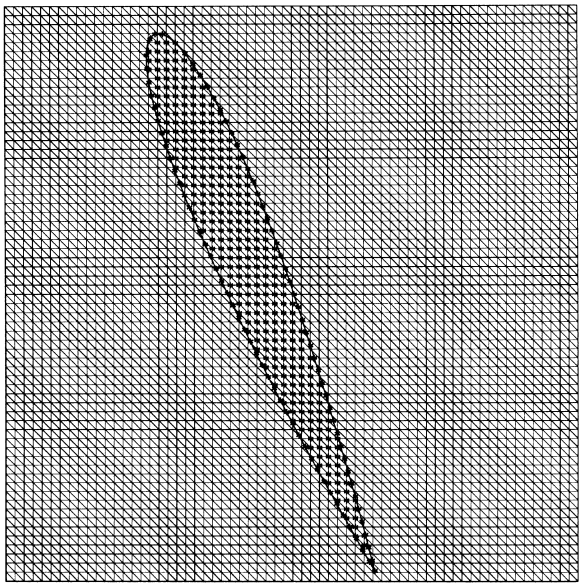

Fig. 5. Part of the velocity mesh and example of mesh points for enforcing the rigid body motion in the NACA0012 airfoil.

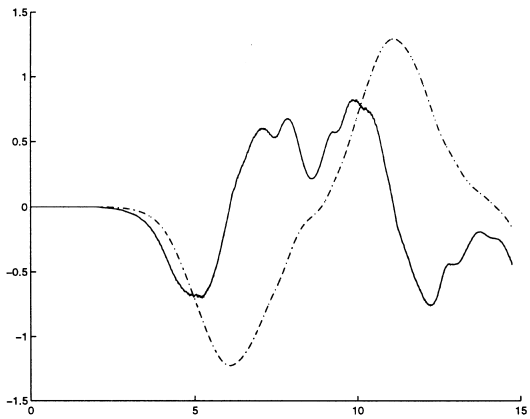

Fig. 6. The histories of the angle (dashed–dotted line) and angular velocity (solid line) of the NACA0012 airfoil at $Re = 807$.

NACA0012 at that time completed by a selected set of points belonging to the boundary of the airfoil (see Fig. 5) and then use a scalar product over $\Lambda_h(t)$ such as the one defined by (3.6).

In the simulation, the number of iterations for the divergence free projection problem (4.5) is 16, the number of iterations for the linearized advection–diffusion problem (4.6) is 2, and the one for the rigid body motion projection varies from 65 to 238. The first two numbers of iterations are almost independent of the mesh size; the last one is quite large and we are working to reduce it via the use of a H^1-scalar product such as the ones defined by (2.50) and (2.51). The histories of the angle and angular velocity of the NACA0012 airfoil are shown in Fig. 6. The flow fields at times $t = 2, 9, 10, 11, 12, 13, 14$ are shown in Figs. 7–13. Before $t = 2$, the NACA0012 airfoil is completely fixed without possible rotation and a steady

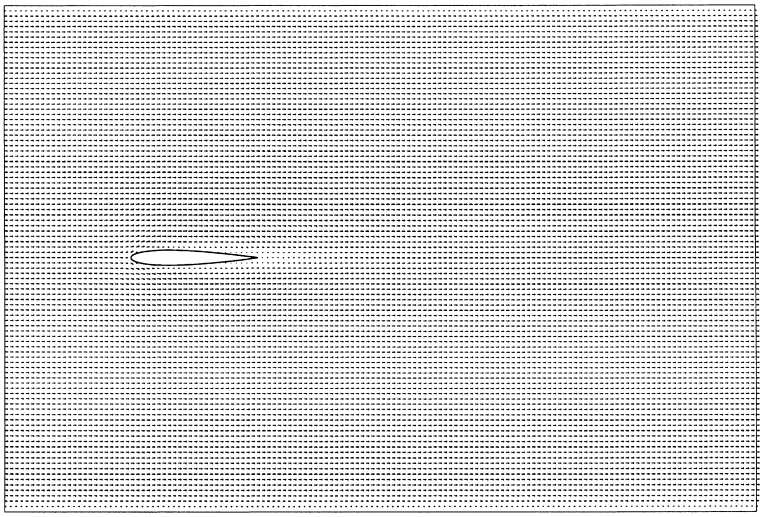

Fig. 7. Flow field around the NACA0012 airfoil at $t = 2$.

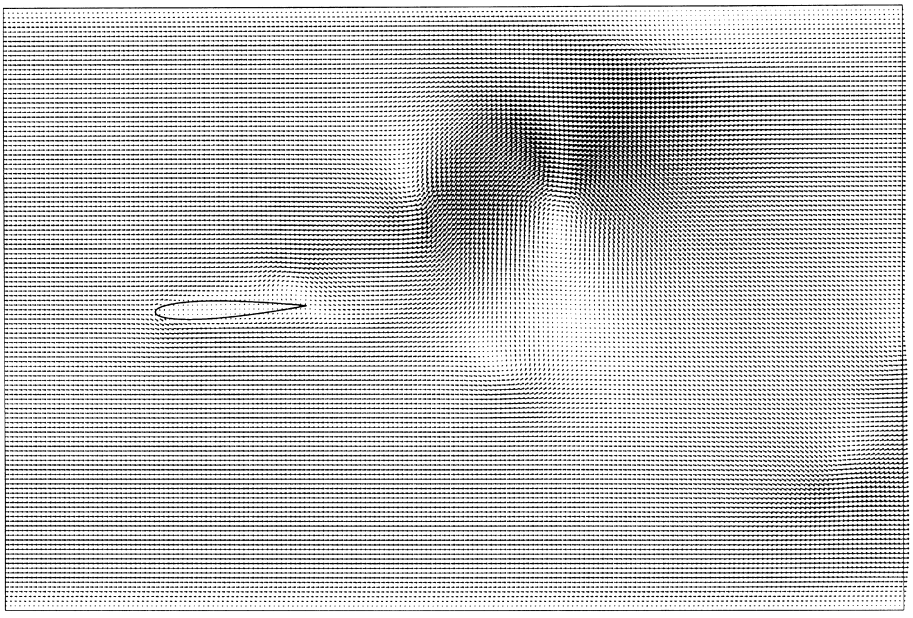

Fig. 8. Flow field around the NACA0012 airfoil at $t = 9$.

flow around it is obtained. After $t = 2$, we allow the NACA0012 airfoil to rotate freely. We observe then that the NACA0012 airfoil oscillates widely from about -70° to 74°.

In the second test case, we have used the same parameters except that the viscosity ν_f is 0.01 (implying that Re is about 101), the time step Δt is 0.001, and the NACA0012 airfoil is completely fixed till $t = 1$. The range of oscillation of the NACA0012 airfoil is much smaller (see Fig. 14) and the eddies created by the

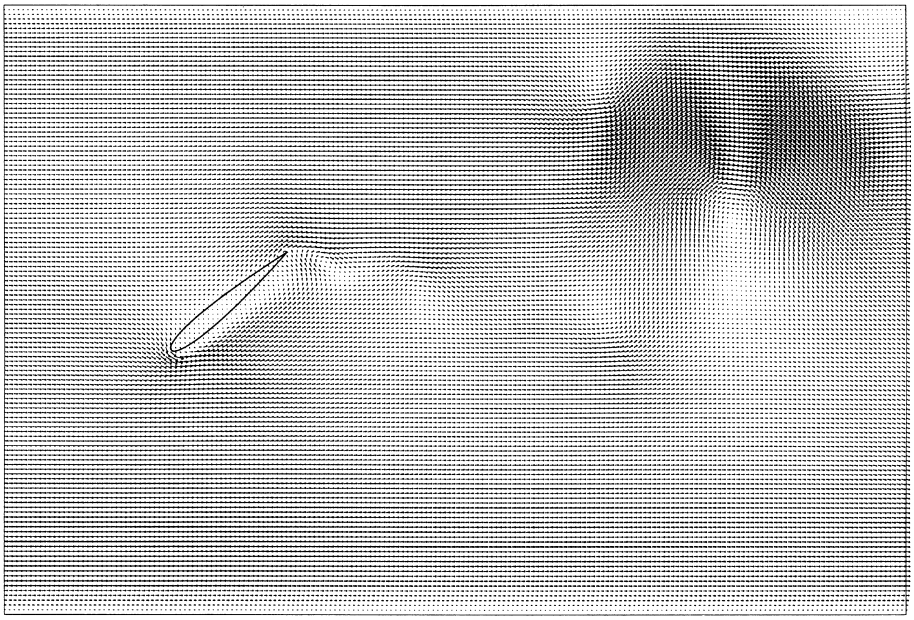

Fig. 9. Flow field around the NACA0012 airfoil at $t = 10$.

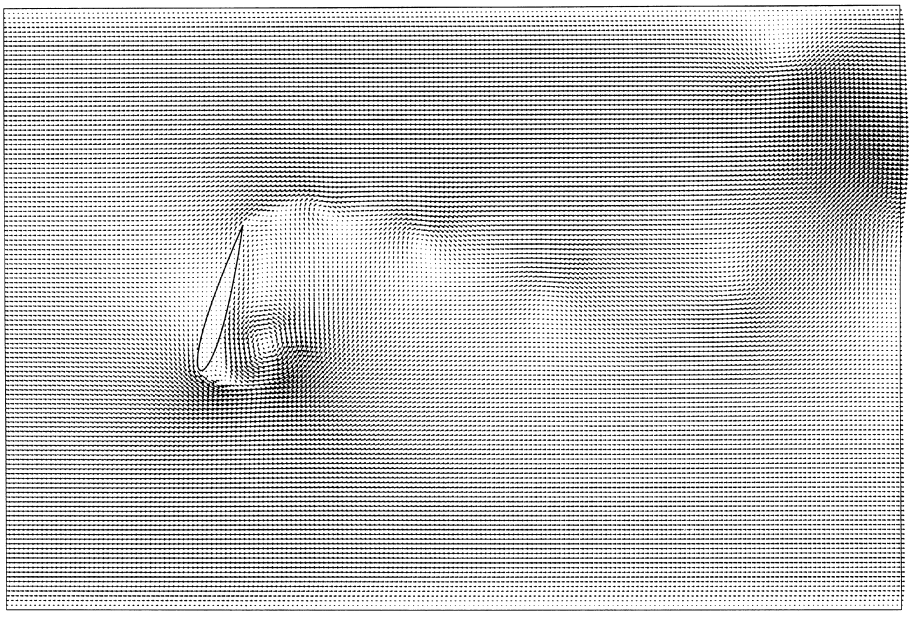

Fig. 10. Flow field around the NACA0012 airfoil at $t = 11$.

oscillation of the airfoil are weaker than those in the case of $Re = 807$. In this case the NACA0012 airfoil intends to keep its broadside perpendicular to the inflow direction, which is a stable position for noncircular particles settling in the channel at small Reynolds number (see Ref. [33] for more details).

Reducing h and Δt brings essentially the same results.

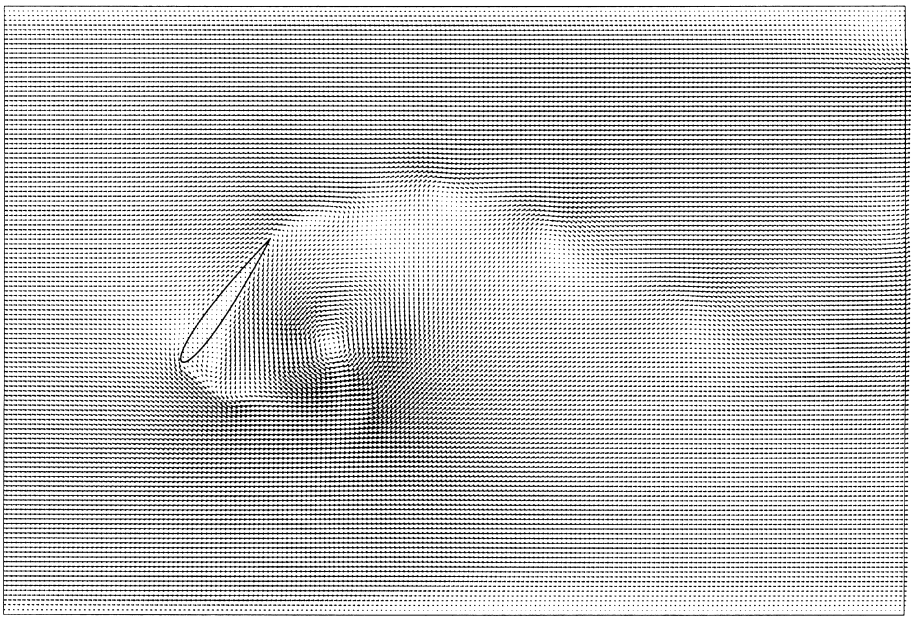

Fig. 11. Flow field around the NACA0012 airfoil at $t = 12$.

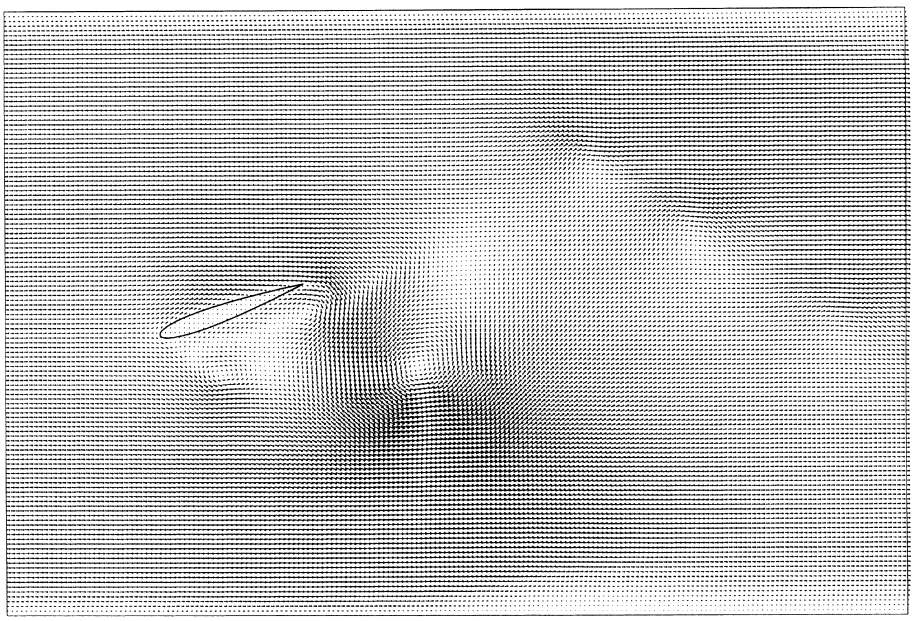

Fig. 12. Flow field around the NACA0012 airfoil at $t = 13$.

6.2. A 1008 particles case

The second test problem that we consider concerns the simulation of the motion of 1008 sedimenting cylinders in the closed channel $\Omega = (0,2) \times (0,4)$. The diameter d of the cylinders is 0.0625 and the position of the cylinders at time $t = 0$ is shown in Fig. 15. The solid fraction in this test case is 38.66%. Initial velocity and angular velocity of the cylinders are $\mathbf{V}_i^0 = \mathbf{0}$, $w_i^0 = 0$ for $i = 1, \ldots, 1008$. The density of the fluid is $\rho_f = 1.0$ and the density of the cylinders is $\rho_s = 1.01$. The viscosity of the fluid is $\nu_f = 0.01$. The initial condition for the fluid flow is $\mathbf{u} = \mathbf{0}$ and $\mathbf{g}_0(t) = \mathbf{0}$ $\forall t \geqslant 0$. The time step is $\Delta t = 0.001$. The mesh size for the velocity field is $h_v = 1/256$ (there are 525,835 nodes). The mesh size for pressure is $h_p = 1/128$ (131,841 nodes). For this many particle case, a fine mesh is required. The parameters for the repulsion force discussed in (5.1) are $\rho = h_v, c = 1$, and ϵ is in the order of 10^{-5}. We have chosen $\alpha = 1$ and $\beta = 0$ in the

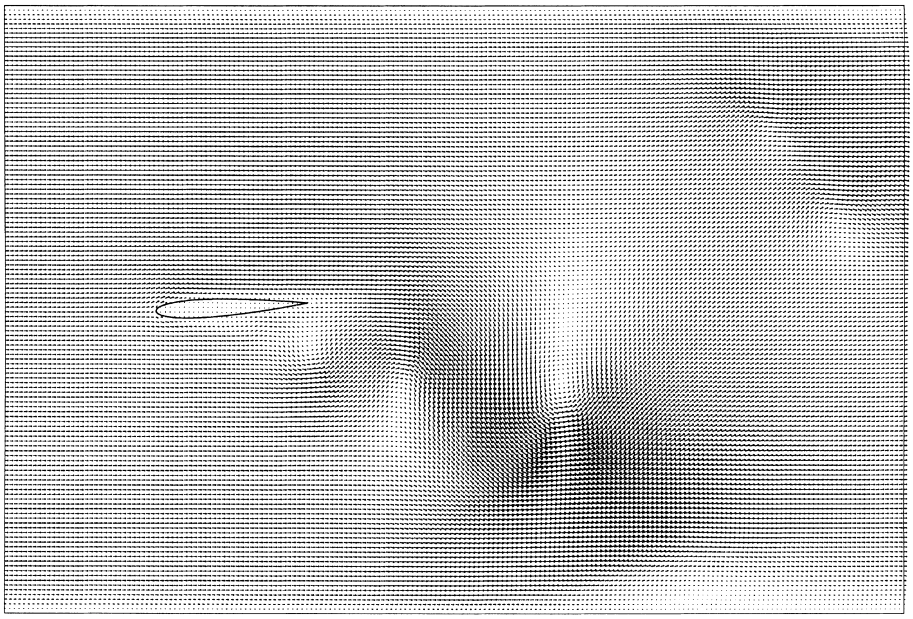

Fig. 13. Flow field around the NACA0012 airfoil at $t = 14$.

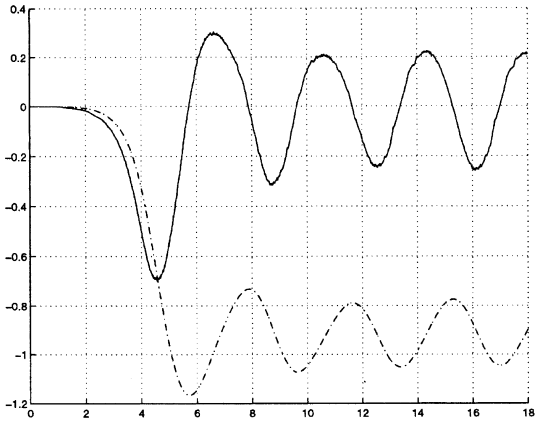

Fig. 14. The histories of the angle (dashed–dotted line) and angular velocity (solid line) of the NACA0012 airfoil at $Re = 101$.

Marchuk–Yanenko scheme. The number of iterations for the divergence free projection problem varies from 12 to 14, the number of iterations for the linearized advection–diffusion problem is 5, and the one for the rigid body motion projection is about 7. Those numbers of iterations are almost independent of the mesh size and of the number of particles. With the finite dimensional spaces defined in Section 3, the

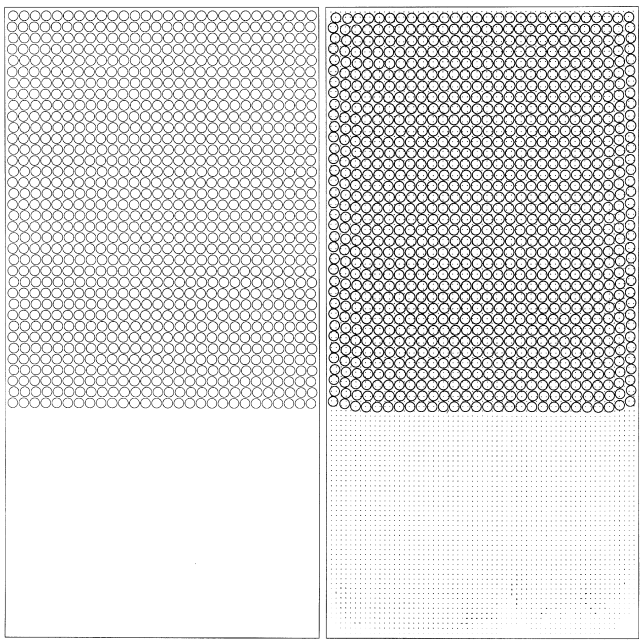

Fig. 15. Sedimentation of 1008 circular particles: $t = 0, 1$ (left to right).

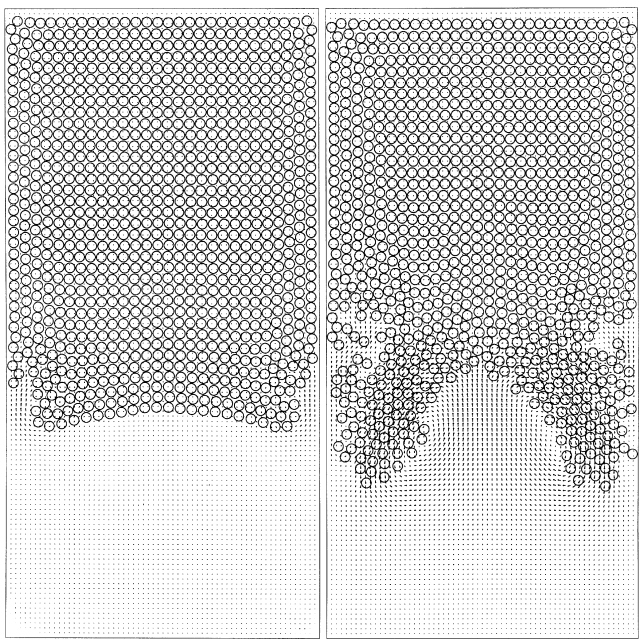

Fig. 16. Sedimentation of 1008 circular particles: $t = 2, 3$ (left to right).

evolution of the 1008 cylinders sedimenting in the closed channel is shown in Figs. 15–19. The maximal particle Reynolds number in the entire evolution is 17.44. The slightly wavy shape of the interface observed at $t = 1$ in Fig. 15 is the typical onset of a Rayleigh–Taylor instability. When t is between 1 and 2, two small eddies are forming close to the left wall and the right wall and some particles are pulling down fast by these

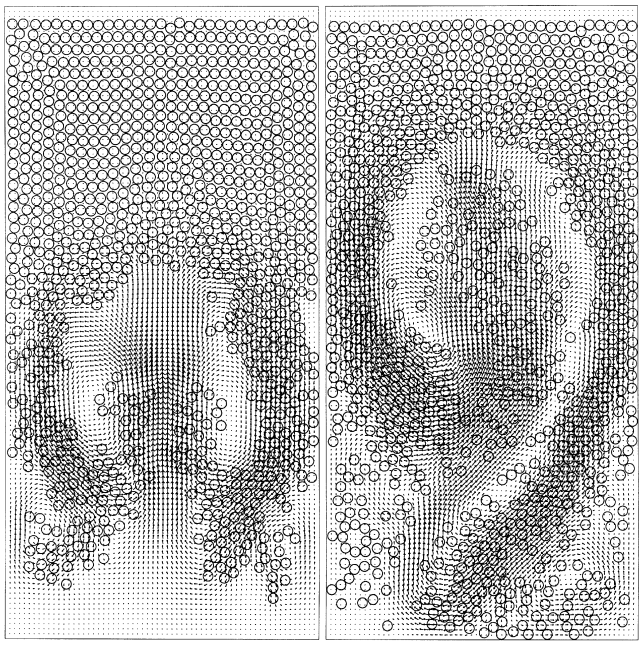

Fig. 17. Sedimentation of 1008 circular particles: $t = 4, 5$ (left to right).

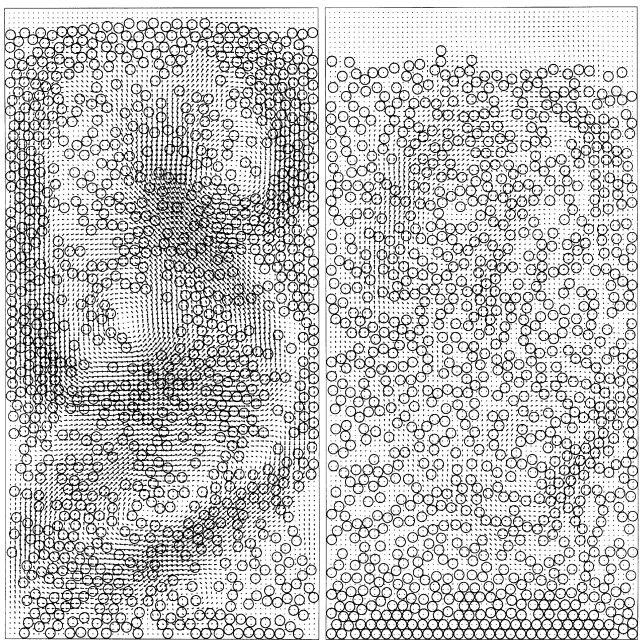

Fig. 18. Sedimentation of 1008 circular particles: $t = 6, 10$ (left to right).

two eddies. Then other two stronger eddies are forming at the lower center of the channel for t between 2 and 4; they push some particles almost to the top wall of the channel. The above figures clearly show a fingering phenomenon, followed by a symmetry breaking. At the end all particles are settled at the bottom of the channel.

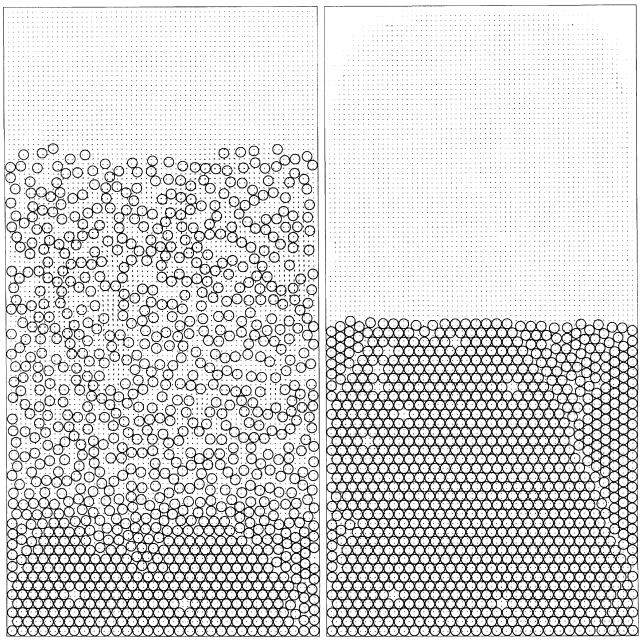

Fig. 19. Sedimentation of 1008 circular particles: $t = 20, 48$ (left to right).

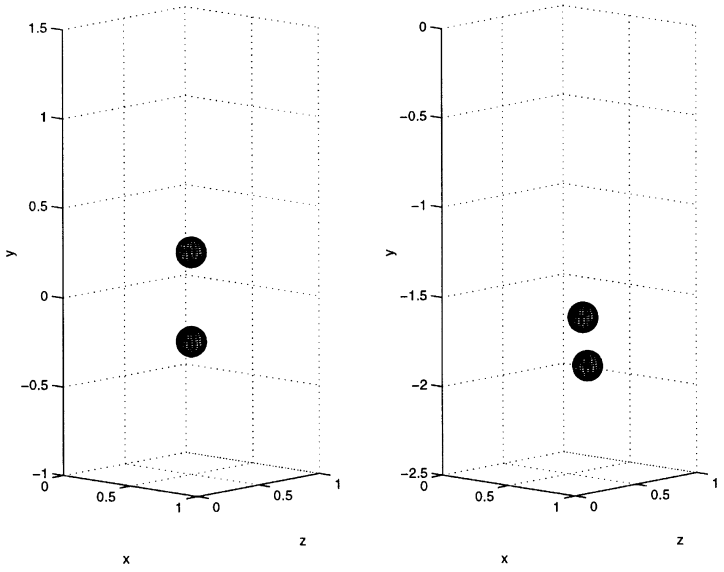

Fig. 20. Particle position at $t = 0, 1$ (left to right).

6.3. A 3-D case with two identical spherical particles

The third test problem that we consider here concerns the simulation of the motion of two sedimenting balls in a rectangular cylinder. A 2-D analogue of this test case problem has been (successfully) investigated in [13] using similar techniques. The initial computational domain is $\Omega = (0,1) \times (-1,1.5) \times (0,1)$, then it moves with the center of the lower ball. The diameter d of the two balls is 1/6 and the position of the balls at time $t = 0$ is shown in Fig. 20. The initial velocity and the angular velocity of the balls are zero. The density of the fluid is $\rho_f = 1.0$ and the density of the balls is $\rho_s = 1.04$. The viscosity of the fluid is $\nu_f = 0.01$. The initial condition for the fluid flow is $\mathbf{u} = 0$. The mesh size for the velocity field is $h_v = 1/60$. The mesh size

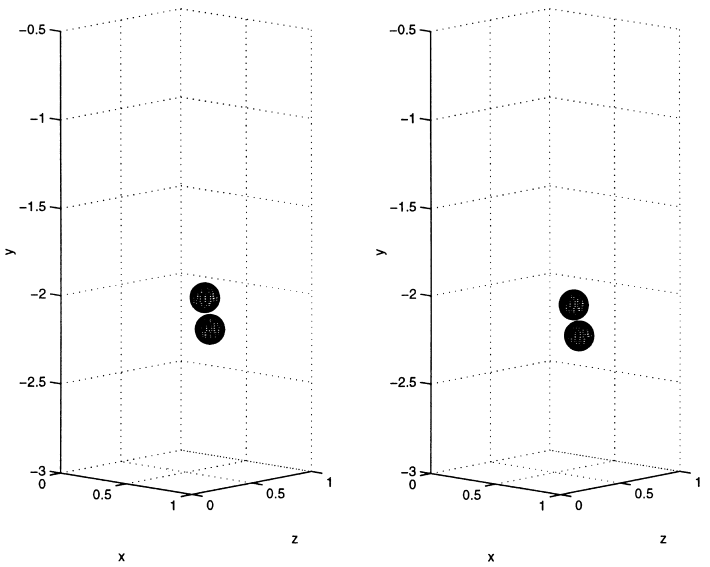

Fig. 21. Particle position at $t = 1.149, 1.169$ (left to right).

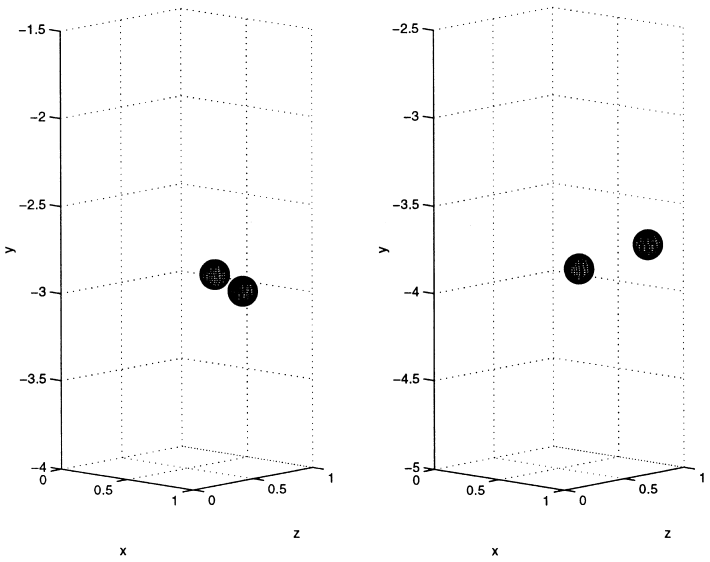

Fig. 22. Particle position at $t = 1.5, 2$ (left to right).

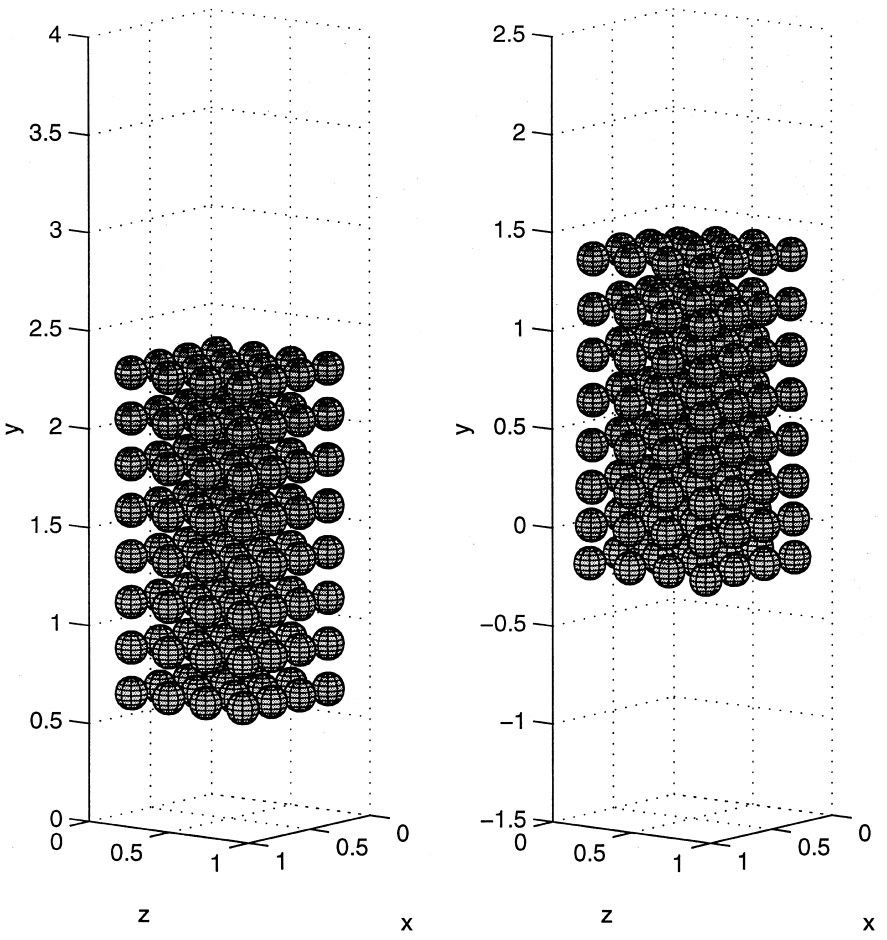

Fig. 23. Particle position at $t = 0, 0.5$ (left to right).

for pressure is $h_p = 1/30$. The time step is $\Delta t = 0.001$. For the parameters discussed in (5.1) we have taken $\rho = 1.5\ h_v, c = 1$, and ϵ is in the order of 10^{-3}. The maximal particle Reynolds number in the entire evolution is 47.57. Figs. 20–22 are drawn by following the position of these two balls. We can see in these figures the fundamental features of two sedimenting balls, i.e., drafting, kissing and tumbling [34]. We observe that a symmetry breaking occurs before the kissing; with a smaller *Re*, this symmetry breaking would occur after the kissing. Using smaller h and Δt brings essentially the same results.

6.4. Sedimentation of 128 balls in three dimension

The last test problem that we consider here concerns the simulation of the motion of 128 sedimenting balls in a rectangular cylinder. The initial computational domain is $\Omega = (0,1) \times (0,4) \times (0,1)$, then it moves with the center of the lowest ball. The diameter d of 128 balls is 1/6 and the position of the balls at time $t = 0$ is shown in Fig. 23. The initial velocity and angular velocity of the balls are zero. The density of the fluid is $\rho_f = 1.0$ and the density of the balls is $\rho_s = 1.14$. The viscosity of the fluid is $\nu_f = 0.01$. The initial condition for the fluid flow is $\mathbf{u} = \mathbf{0}$. The mesh size for the velocity field is $h_v = 1/60$ (896,761 nodes). The mesh size for pressure is $h_p = 1/30$ (116,281 nodes). The time step $\Delta t = 0.002$. For the parameters discussed in (5.1) we have taken $\rho = 1.5h_v$, $c = 1$, and ϵ is in the order of 10^{-5}. The maximal particle Reynolds number in the entire simulation is about 98. In Figs. 23 and 24, we can see those balls falling, and later drafting, kissing, and tumbling. This simulation demonstrates the potential of distribution Lagrange multiplier method.

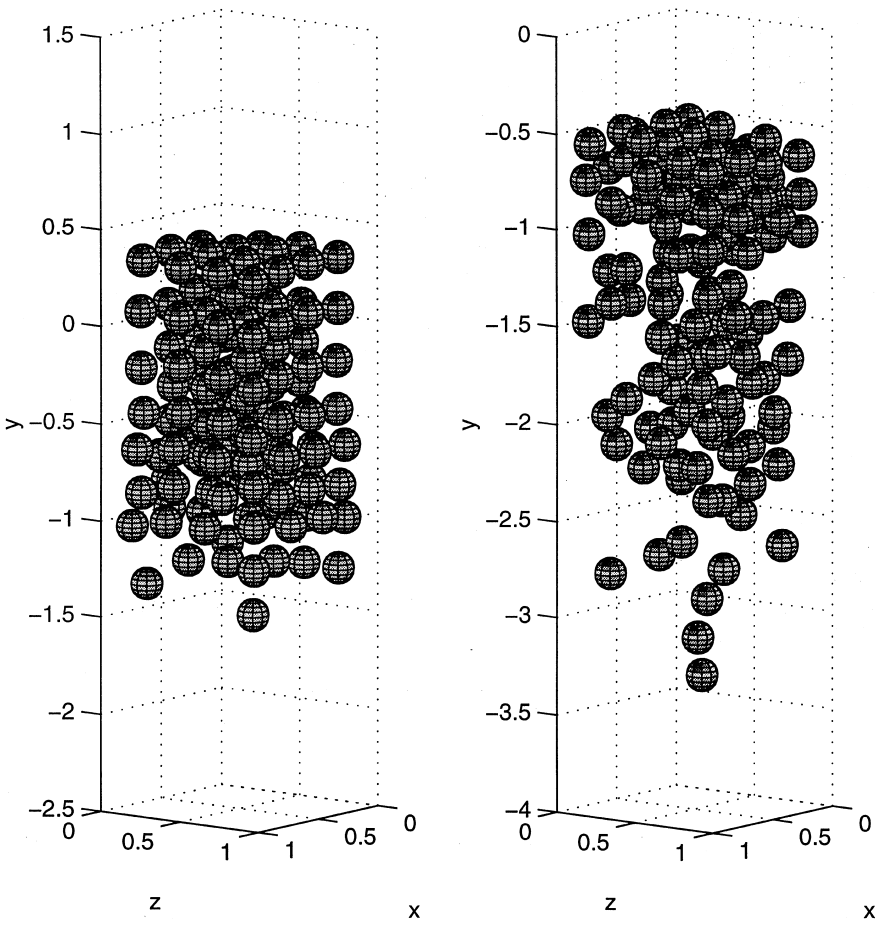

Fig. 24. Particle position at $t = 1, 1.5$ (left to right).

7. Conclusion

We have presented in this article a distributed Lagrange multiplier based fictitious domain method for the simulation of flow with moving boundaries. Compared to the one discussed earlier in [13], it allows the simulation of fairly complicated flow phenomena, such as particulate flow, including sedimentation. Some preliminary experiments have shown the potential of this method for the direct simulation of fluidization which is in some sense the inverse phenomenon of sedimentation; the results already obtained look promising. Other goals include: 3-D particulate flow with large number of particles of different sizes and shapes, particulate flow for viscoelastic liquids such as Oldroyd B and so on.

Acknowledgements

We acknowledge the helpful comments and suggestions of E.J. Dean, V. Girault, J. He, Y. Kuznetsov, B. Maury, and G. Rodin and also the support of NEC concerning the use of an SX-3 supercomputer. We acknowledge also the support of the NSF under HPCC Grand Challenge Grant ECS-9527123, NSF (Grants DMS 8822522, DMS 9112847, DMS 9217374), Dassault Aviation, DRET (Grant 89424), DARPA (Contracts AFOSR F49620-89-C-0125, AFOSR-90-0334), the Texas Board of Higher Education (Grants 003652156ARP and 003652146ATP) and the University of Houston (PEER grant 1-27682).

References

[1] R. Glowinski, T.-W. Pan, J. Périaux, A fictitious domain method for Dirichlet problem and applications, Comput. Meth. Appl. Mech. Eng. 111 (1994) 283–303.
[2] R. Glowinski, T.-W. Pan, J. Périaux, A fictitious domain method for external incompressible viscous flow modeled by Navier–Stokes equations, Comput. Meth. Appl. Mech. Eng. 112 (1994) 133–148.
[3] R. Glowinski, T.-W. Pan, J. Périaux, A Lagrange multiplier/fictitious domain method for the Dirichlet problem. Generalization to some flow problems, Japan J. Industrial Appl. Math. 12 (1995) 87–108.
[4] R. Glowinski, T.-W. Pan, J. Périaux, Fictitious domain methods for incompressible viscous flow around moving rigid bodies, in: J.R. Whiteman (Ed.), The Mathematics of Finite Elements and Applications, Highlight 1996, Wiley, Chichester, England, 1997 pp. 155–174.
[5] R. Glowinski, T.-W. Pan, J. Périaux, A Lagrange multiplier/fictitious domain method for the numerical simulation of incompressible viscous flow around moving rigid bodies (I): the case where the rigid body motions are known a priori, C. R. Acad. Sci. Paris, 324 (1997) 361–369.
[6] R. Glowinski, T.W. Pan, J. Périaux, Distributed Lagrange multiplier methods for incompressible viscous flow around moving rigid bodies, Comput. Meth. Appl. Mech. Eng. 151 (1998) 181–194.
[7] A. Johnson, T. Tezduyar, 3-D Simulation of fluid-rigid body interactions with the number of rigid bodies reaching 100, University of Minnesota, AHPCRC preprint, 1996, pp. 96–037.
[8] C.S. Peskin, Numerical analysis of blood flow in the heart, J. Comput. Phys. 25 (1977) 220–252.
[9] C.S. Peskin, D.M. McQueen, Modeling prosthetic heart valves for numerical analysis of blood flow in the heart, J. Comput. Phys. 37 (1980) 113–132.
[10] C.S. Peskin, Lectures on mathematical aspects of physiology, Lectures in Appl. Math. 19 (1981) 69–107.
[11] R.J. LeVeque, Z. Li, The immersed interface method for elliptic equations with discontinuous coefficients and singular sources, SIAM J. Numer. Anal. 31 (1994) 1019–1044.
[12] R.J. LeVeque, Z. Li, Immersed interface methods for Stokes flow with elastic boundaries or surface tension, SIAM J. Sci. Comput. 18 (1997) 709–735.
[13] R. Glowinski, T.W. Pan, T. Hesla, D.D. Joseph, J. Périaux, A distributed Lagrange multiplier/fictitious domain method for particulate flows, Internat. J. Multiphase Flow 25 (1999) 755–794.
[14] B.A. Maury, A many-body lubrication model, C. R. Acad. Sci., Paris t. 325, Série I, 1997, pp. 1053–1058.
[15] T.I. Hesla, The dynamical simulation of 2-D fluid/rigid body systems, unpublished notes, 1991.
[16] H.H. Hu, Direct simulation of flows of solid–liquid mixtures, Internat. J. Multiphase Flow 22 (1996) 335–352.
[17] F. Bertrand, P.A. Tanguy, F. Thibault, A 3-D fictitious domain method for incompressible fluid flow problem, Internat. J. Numer. Meth. Fluids 25 (1997) 719–736.
[18] F. Brezzi, M. Fortin, Mixed and Hybrid Finite Element Methods, Springer, New York, 1991.
[19] J.E. Roberts, J.M. Thomas, Mixed and Hybrid Methods, in: P.G. Ciarlet, J.L. Lions (Eds.), Handbook of Numerical Analysis, vol. II, North-Holland, Amsterdam, 1991, pp. 523–639.
[20] A.J. Chorin, A numerical method for solving incompressible viscous flow problem, J. Comput. Phys. 2 (1967) 12–26.
[21] A.J. Chorin, On the convergence and approximation of discrete approximation to the Navier–Stokes equations, Math. Comput. 23 (1968) 341–353.
[22] A.J. Chorin, Numerical study of slightly viscous flow, J. Fluid Mech. 57 (1973) 785–796.
[23] R. Glowinski, O. Pironneau, Finite element methods for Navier–Stokes equations, Ann. Rev. Fluid Mech. 24 (1992) 167–204.
[24] S. Turek, A comparative study of time-stepping techniques for the incompressible Navier–Stokes equations: from fully implicit nonlinear schemes to semi-implicit projection methods, Internat. J. Numer. Math. Fluids 22 (1996) 987–1011.
[25] G.I. Marchuk, Splitting and alternate direction methods, in: P.G. Ciarlet, J.L. Lions (Eds.), Handbook of Numerical Analysis, vol. I, North-Holland, Amsterdam, 1990, pp. 197–462.
[26] E. Dean, R. Glowinski, A wave equation approach to the numerical solution of the Navier–Stokes equation for incompressible viscous flow, C.R. Acad. Sci. Paris, t. 325, Série I, 1997, pp. 783–791.
[27] E. Dean, R. Glowinski, T.-W. Pan, A wave equation approach to the numerical simulation of incompressible viscous fluid flow modeled by the Navier–Stokes equations, in: J. De Santo (Ed.), Mathematical and numerical aspects of wave propagation, SIAM, Philadelphia, 1998, pp. 65–74.
[28] R. Glowinski, Numerical Methods for Nonlinear Variational Problems, Springer, New York, 1984.
[29] M. Fortin, R. Glowinski, Augmented Lagrangian Methods, North-Holland, Amsterdam, 1983.
[30] R. Glowinski, P. LeTallec, Augmented Lagrangian and Operator-Splitting Methods in Nonlinear Mechanics, SIAM, Philadelphia, PA, 1989.
[31] N. Kikuchi, T.J. Oden, Contact Problems in Elasticity, SIAM, Philadelphia, PA, 1988.
[32] E.J. Dean, R. Glowinski, Y.M. Kuo, M.G. Nasser, On the discretization of some second order in time differential equations, Applications to nonlinear wave problems, in: A.V. Balakrishnan (Ed.), Computational Techniques in Identification and Control of Flexible Flight Structures, Optimization Software, Inc., Los Angeles, 1990, pp. 199–246.
[33] H. Hu, D.D. Joseph, A.F. Fortes, Experiments and direct simulation of fluid particle motions, Internat. Vid. J. Eng. Res. 2 (1992) 17.
[34] A.F. Fortes, D.D. Joseph, T.S. Lundgren, Nonlinear mechanics of fluidization of beds of spherical particles, J. Fluid Mech. 177 (1987) 467–483.